Increased circulating levels of Factor H-Related Protein 4 are strongly associated with age-related macular degeneration

Valentina Cipriani[1,2,3,4,16,*], Laura Lorés-Motta[5,16], Fan He[6], Dina Fathalla[7], Viranga Tilakaratna[6], Selina McHarg[6], Nadhim Bayatti[6], İlhan E. Acar[5], Carel B. Hoyng[5], Sascha Fauser[8,9], Anthony T. Moore[1,2,10], John RW Yates[1,2,11], International Age-related Macular Degeneration Genomics Consortium (IAMDGC), Eiko K de Jong[5], B. Paul Morgan[7,17], Anneke I. den Hollander[5,12,17], Paul N. Bishop[6,13,17], Simon J. Clark[6,14,15, 17,*]

[1]UCL Institute of Ophthalmology, University College London, London, EC1V 9EL, UK.

[2]Moorfields Eye Hospital NHS Foundation Trust, London, EC1V 2PD, UK.

[3]UCL Genetics Institute, University College London, London, WC1E 6BT, UK.

[4]William Harvey Research Institute, Clinical Pharmacology, Queen Mary University of London, London, EC1M 6BQ, UK.

[5]Department of Ophthalmology, Donders Institute for Brain, Cognition and Behaviour, Radboud university medical centre, Nijmegen, 6525 HR, the Netherlands.

[6]Division of Evolution and Genomic Sciences, School of Biological Sciences, Faculty of Biology Medicine and Health, University of Manchester, Oxford Road, Manchester, M13 9PT, UK.

[7]Systems Immunity URI, Division of Infection and Immunity, and UK DRI Cardiff, School of Medicine, Cardiff University, Cardiff, CF14 4XN, UK.

[8]Department of Ophthalmology, University Hospital of Cologne, Cologne, 50924, Germany.

[9]Roche Pharma Research and Early Development, F. Hoffmann-La Roche Ltd, Basel, CH-4070, Switzerland.

[10]Ophthalmology Department, University of California San Francisco, San Francisco, California.

[11]Department of Medical Genetics, University of Cambridge, Cambridge, CB2 0QQ, UK.

[12]Department of Human Genetics, Donders Institute for Brain, Cognition and Behaviour, Radboud university medical centre, Nijmegen, 6525 HR, the Netherlands.

[13]Manchester Royal Eye Hospital, Manchester University NHS Foundation Trust, Manchester Academic Health Science Centre, M13 9WL, UK.

[14]The Lydia Becker Institute of Immunology and Inflammation, Faculty of Biology, Medicine and Health, University of Manchester, Manchester, UK

[15]Current address: Research Institute of Ophthalmology, Department of Ophthalmology, Eberhard Karls University of Tübingen, 72076 Tübingen, Germany

[16]These authors contributed equally to this work.

[17]These authors jointly supervised this work.

[*]Correspondence should be addressed to: V.C. (v.cipriani@qmul.ac.uk) or S.J.C. (simon.clark@uni-tuebingen.de)

Abstract

Age-related macular degeneration (AMD) is a leading cause of blindness. Genetic variants at the chromosome 1q31.3 encompassing the complement factor H (*CFH*, FH) and *CFH* related genes (*CFHR1-5*) are major determinants of AMD susceptibility, but their molecular consequences remain unclear. We demonstrate that FHR-4 plays a prominent role in AMD pathogenesis. We show that systemic FHR-4 levels are elevated in AMD (P-value=7.1×10^{-6}), whereas no difference is seen for FH. Furthermore, FHR-4 accumulates in the choriocapillaris, Bruch's membrane and drusen, and can compete with FH/FHL-1 for C3b binding, preventing FI-mediated C3b cleavage. Critically, the protective allele of the strongest AMD-associated *CFH* locus variant rs10922109 has the highest association with reduced FHR-4 levels (P-value=2.2×10^{-56}), independently of the AMD-protective *CFHR1–3* deletion, and even in those individuals that carry the high-risk allele of rs1061170 (Y402H). Our findings identify FHR-4 as a new molecular player contributing to complement dysregulation in AMD.

Introduction

Age-related macular degeneration (AMD) is the most common cause of vision loss in Western societies[1]. Soft drusen are an early sign of AMD. These deposits form within Bruch's membrane (BrM) underneath the retinal pigment epithelium (RPE) basement membrane and contain apolipoprotein B and E, cholesterol-rich lipoproteins that are thought to be derived from the RPE[2]. In addition, they contain a variety of other proteins, with complement proteins being a prominent component[3]. This early stage of disease can then progress to late AMD, manifesting as either geographic atrophy ('dry' AMD) or choroidal neovascularisation ('wet' AMD)[4].

AMD has a strong genetic basis; associations with 45 common single nucleotide polymorphisms (SNPs) and 7 rare variants across 34 genetic loci have been reported in the largest genome-wide association study (GWAS) to date, explaining ~34% of AMD risk[5]. Many of these variants reside in genes encoding complement system components, particularly those encoded at the Regulators of Complement Activation (RCA) locus on chromosome 1q31.3, including factor H (FH; *CFH)* and FH related 1-5 (*CFHR1-5*)[6,7]. Common SNPs within *CFH*, including rs1061170 encoding a tyrosine to histidine substitution at position 402 (Y402H), were first identified as major susceptibility variants for AMD[8-11]. The recent largest GWAS established 8 independent signals (4 common variants, 4 rare) over 578 Mb of the RCA locus[5]. Except for the highly penetrant *CFH* missense variant R1210C[12] and synonymous variant rs35392876 in *CFH*, all variants are non-coding: 4 intronic in *CFH* (2), *CFHR5* (1) and *KCNT2* (1) and 2 intergenic (8kb upstream *CFH*/35kb downstream *KCNT2*; 14kb downstream *CFHR1*/156kb upstream *CFHR4*). The role of these genes in the pathogenesis of AMD is unclear.

The *CFH* gene encodes FH and its smaller splice variant, FH-like 1 (FHL-1)[13,14]. FH is the main plasma complement regulator, but FHL-1 predominates in BrM and choriocapillaris[6,15].

Whilst FH/FHL-1 downregulate complement activation in plasma and on surfaces, the FHR proteins can compete with FH/FHL-1 for surface and ligand binding, thus disrupting their negative regulatory function and facilitate local activation[16,17] (see Figure 3 of reference 17 for an explanatory diagram of *CFH* and *CFHR* genes and the structures of FH, FHL-1 and FHR proteins). However, due to the extremely high level of sequence homology shared by all of the FHR proteins[17] it has thus far remained difficult to investigate their individual tissue expression patterns. Rare AMD-associated coding variants in *CFH* and their functional consequences directly implicate FH in the pathogenesis of AMD[5,12,18-22]. The molecular basis of the association of FH/FHL-1 402H variant to AMD pathology has been reported to involve altered binding to heparan sulfate, C-reactive protein or malondialdehyde, impacting local complement activation and subretinal inflammation[23-26]. Downstream of *CFH*, a common ~84 kb deletion of *CFHR3* and *CFHR1* and a rare ~120 kb deletion encompassing *CFHR1* and *CFHR4* are associated with reduced AMD risk, supporting the hypothesis that multiple genes at the locus may be involved in AMD[27-34]. In line with the genetic findings, dysregulation of the complement system in the eye and blood has been reported in the early stages of AMD predominating in the extracellular matrix surrounding the fenestrated capillaries of the choriocapillaris that underlies Bruch's membrane[35-38].

A recent GWAS identified an intronic variant in *CFHR4* that associated with increased systemic complement activation and AMD risk[39]. Furthermore, it has recently been reported that the top AMD-associated *CFH* variant rs10922109[5] is associated with altered *CFHR4* expression in liver[40]. Taken together these studies propose that, as well as FH, FHR-4 may also be involved in AMD. Having recently generated a novel, specific monoclonal antibody against FHR-4, we investigated, using a combination of biochemical, immunohistochemical and genetic approaches, whether FHR-4 directly impacts AMD pathogenesis. We show, in two large, independent cohorts,

that blood FHR-4 levels are elevated in AMD patients compared to controls. FHR-4 is present in areas of pathology in AMD retina, co-localising with complement activation products. *In vitro* functional analyses show that FHR-4 binds C3 fragments and competes out the binding of the regulatory proteins FH and FHL-1. Genetic association analyses show that several of the established AMD risk variants at the *CFH* locus are associated with FHR-4 levels in blood, a finding strongly supported by haplotype association analyses. Taken together, our findings implicate FHR-4 as a key driver of complement dysregulation in the AMD retina and identify FHR-4 as a new potential therapeutic target in AMD.

Results

Systemic FHR-4 levels are elevated in advanced AMD cases

Systemic FHR-4 concentrations were measured in plasma and serum samples of 484 late AMD patients (geographic atrophy and/or choroidal neovascularization) and 522 phenotyped controls, collected within two independent AMD studies (Cambridge and EUGENDA; Table 1). AMD patients had significantly elevated FHR-4 levels compared to controls, in each study separately (β=0.18 and P-value=0.016 for Cambridge and β=0.19 and P-value=1.7×10^{-4} for EUGENDA) and in the two-cohort meta-analysis (β=0.19, 95% confidence interval (CI) 0.11 – 0.27 and P-value=7.1×10^{-6}) (Table 1 and Fig. 1A). Association of FHR-4 levels stratified by type of end-stage disease, i.e., CNV only and GA only, were additionally performed. These analysis showed comparable estimates in both cohorts (CNV only: β=0.15 and P-value=0.068 for Cambridge and β=0.18 and P-value=0.001 for EUGENDA; GA only: β=0.20 and P-value=0.099 for Cambridge and β=0.45 and P-value=0.008 for EUGENDA) and in the meta-analysis (CNV only: β=0.17, CI 0.09 – 0.26 and P-value=9.3×10^{-5}; GA only: β=0.28, CI 0.09 – 0.47 and P-value=0.004), with wider CIs for the GA only group reflecting the smaller sample size (62 GA only cases in Cambridge and 10 GA only cases in EUGENDA). The overall adjusted odds ratio (OR) of advanced disease for an FHR-4 increase of 1 standard deviation was 1.37 (CI =1.19–1.58; P-value=1.8×10^{-5}) (Supplementary Fig. 1A). We also measured systemic FH levels and found no significant difference between patients and controls (P-values 0.959, 0.535 and 0.704 for Cambridge, EUGENDA and meta-analysis, respectively; Table 1, Fig. 1B and Supplementary Fig. 1B).

130 ***CFHR4 is expressed in liver but not the eye***

131 We found no evidence of transcription of the *CFHR4* gene in primary human RPE cells by rtPCR
132 (Supplementary Fig. 2A). Analysis of the Gene Expression Omnibus datasets
133 (https://www.ncbi.nlm.nih.gov/geo) confirmed absence of *CFHR4* transcription in the
134 neurosensory retina, RPE and choroid using Affymetrix U133plus2 human genome arrays,[41]
135 Affymetrix Human Exon 1.0 ST arrays,[42,43] or RNA sequencing[44,45] (Supplementary Fig. 2B-F).
136 Analysis of gene expression across 53 human tissues from the Genotype-Tissue Expression project
137 (https://www.ebi.ac.uk/gxa/home)[46] demonstrated that *CFHR4* expression was restricted to the
138 liver (Supplementary Fig. 2G).

139

140 ***FHR-4 in the choriocapillaris is associated with complement activation***

141 Immunostaining demonstrated that FHR-4 accumulates in the intercapillary septa, the extracellular
142 matrix (ECM) between the fenestrated capillaries of the choriocapillaris (Fig. 2A-C), and within
143 BrM (Fig. 2C). Diffusion experiments demonstrated that FHR-4 does not completely transit this
144 ECM (Supplementary Fig. 3). Drusen, a hallmark of AMD, were strongly positive for FHR-4
145 antibody labeling (Fig. 2D). C3b also localized to the choriocapillaris intercapillary septa and
146 appeared to co-localise with FHR-4 (Fig. 2E). FHR-4 is reported to bind C3b and stabilize the C3
147 convertase[47,48]. We confirmed that FHR-4 binds immobilized C3b (Fig. 2F) and demonstrated that
148 FHR-4 competes with the negative regulators, FH and FHL-1, for binding immobilized C3b (Fig.
149 2G). The consequences of this were modelled *in vitro* employing C3b α-chain cleavage assays
150 (Fig. 2H and Supplementary Fig. 4). C3b was incubated with FHL-1 and factor I (FI) titrated to
151 give ~80% C3b α-chain cleavage; FHR-4 inhibited α-chain cleavage in a dose-dependent manner;
152 a 2.5-fold molar excess of FHR-4 over FHL-1 caused 50% reduction in cleavage (Fig. 2I).

153

154 ***CFH locus AMD risk variants associate with systemic FHR-4 levels***

155 The International AMD Genomics Consortium (IAMDGC) GWAS[5] reported 8 independently
156 associated variants at the *CFH* locus (Fig. 3A and Supplementary Data 1). We repeated single-
157 variant association analyses with AMD in the Cambridge and EUGENDA samples (originally part
158 of the IAMDGC dataset) and observed all ORs with the same direction and similar magnitude as
159 in IAMDGC at all variants, except for rare variant rs191281603 (Supplementary Data 1).

160 We hypothesised that one or several of the established AMD risk variants at the *CFH* locus
161 are associated with increased systemic FHR-4 levels. The rare *CFH* variant R1210C,[12] present
162 heterozygously in a single case from the Cambridge cohort (with corresponding values of FHR-4
163 and FH levels equal to 5.7 and 296.4, respectively), was excluded from this analysis. The top
164 (rs10922109, 1.1), second (rs570618, 1.2; proxy for Y402H), fifth (rs187328863, 1.5) and sixth
165 (rs61818925, 1.6) IAMDGC hits at the *CFH* locus showed strong associations with FHR-4 levels
166 (after Bonferroni correction for multiple testing), with direction of allelic effect on levels
167 concordant with that on disease for all variants (Table 2, Fig. 3B, Supplementary Data 2 and
168 Supplementary Fig. 5). The strongest allelic effect on FHR-4 levels was seen at the top IAMDGC
169 variant rs10922109, with β=-0.42 and P-value=2.2×10^{-56} for the minor allele A associated with
170 decreased disease risk. In the Cambridge and EUGENDA cohorts, respectively, this finding
171 translates into (back-log transformed) FHR-4 levels expressed as geometric mean values [95%
172 CIs] equal to 7.7 ug/ml [7.0-8.5] and 8.5 ug/ml [7.9-9.1] in *CC* genotype individuals, 5.5 ug/ml
173 [5.0-6.1] and 6.0 ug/ml [5.7-6.4] in *AC* genotype individuals and 3.2 ug/ml [2.5-4.0] and 3.6 ug/ml
174 [3.3-3.9] in *AA* genotype individuals. Analogous single-variant association analyses with FH levels
175 revealed a significant association only at rs10922109 and rs61818925 with much smaller effect

size (β=0.03 and β=-0.03, respectively) (Table 2, Supplementary Data 2 and Supplementary Fig. 5).

To assess whether genetic variants at loci other than *CFH* associated with systemic FHR-4 levels, we performed a subsidiary (hypothesis-free) GWAS meta-analysis of FHR-4 levels. A single ~1 Mb region spanning the extended *CFH* locus (chr1q31.3:196,240,335–197,281,307) showed genome-wide significant ($P \leq 5x10^{-8}$) associations with FHR-4 levels (Fig. 4A, Supplementary Fig. 6A and Supplementary Data 3 and Supplementary Data 4). The top signal rs7535263 is in tight linkage disequilibrium (LD) (R^2=0.98, D'=1.00) with the top IAMDGC variant rs10922109 (1.1) (regional plot in Fig. 4A, Supplementary Data 5; OR=0.11, P-value=$1.7x10^{-612}$ in IAMDGC). Analogous GWAS meta-analysis of FH levels also revealed a single genome-wide significant association confined to variants in tight LD in a ~150 kb region at the *CFH* locus (chr1q31.3:196,674,714-196,825,287; including rs6677604, a proxy for the previously reported AMD protective *CFHR1-3* deletion[29]) (Fig. 4B, Supplementary Fig. 6B, Supplementary Data 6, Supplementary Data 7 and Supplementary Data 8), but effect on FH levels was limited (β=-0.10, P-value=$2.4x10^{-11}$ at the top variant rs74696321). Notably, the intronic AMD risk variant rs6685931 in *CFHR4* (LD with rs10922109: R^2=0.43, D'=0.96), associated with complement activation in the recent GWAS,[39] was strongly associated with levels of FHR-4 (β=0.28, P-value=$2.3x10^{-25}$), but not FH (β=0.005, P-value=0.607).

CFH locus haplotypes strongly associate with AMD and FHR-4 levels

To assess the combined effect of variants at the *CFH* locus, we carried out association analyses of the haplotypes formed by the 7 *CFH* variants considered in our study with AMD and FHR-4/FH levels; we included rs6677604 as proxy for the *CFHR1-3* deletion[29] to assess its influence on FHR-

4/FH levels. The rare *CFHR1-4* deletion[33,34] was present heterozygously in 3 controls and 1 advanced AMD patient and was not included in this analysis. Haplotype associations with AMD were also assessed in the whole IAMDGC dataset.[5]

We observed 9 common haplotypes with overall frequency ≥ 1% (Fig. 5B and Supplementary Data 9). The most frequent haplotype CTTGCCGC (H1; controls 32%, cases 49% in IAMDGC) that carries the disease risk allele of the proxy for Y402H (1.2) was used as reference. Common H2-H5 and rarer H7 haplotypes carried significantly lower AMD risk than H1, while rarer H6 (TTTGCCGC) and H9 (CTTGCTGC) carried higher risk than H1; H8 (CTTGCCTC) did not show a significantly different risk from H1 (Fig. 5A and Supplementary Data 9). Similar OR estimates were observed in our two-cohort meta-analysis (Fig. 5A and Supplementary Data 9).

Haplotypes H2 (CTGGACTC) and H3 (CTGAACGC) strongly associated with decreased FHR-4 levels and carry independent effects with no overlapping CIs (β=-0.49, P-value=1.7×10^{-44} and β=-0.25, P-value=4.4×10^{-10}, respectively) (Fig. 5A and Supplementary Data 9). While both haplotypes carry the FHR-4 lowering/AMD protective alleles A of rs10922109 (1.1) and G of rs570618 (1.2), H2 carries the FHR-4 lowering/AMD protective allele T of rs61818925 (1.6) and H3 carries the FHR-4 lowering/AMD protective allele A of rs6677604, tag for the AMD protective *CFHR1-3* deletion. Neither of the haplotypes showed a more significant association with FHR-4 levels than the meta-analysis single-variant associations (Table 2). Analogous haplotype association analyses with FH levels revealed a significant association only at H2 (after Bonferroni correction) with small effect (β=0.07, P-value=3.3×10^{-6}). Results for the diplotype (haplotype pair) association analyses are shown in Supplementary Data 10 and Supplementary Fig. 7. Remarkably, among the genotypes that contain one copy of H1 (Y402H), diplotypes H1:H2, H1:H3 and H1:H7 showed a significantly lower AMD risk (OR=0.33, P-value=5.3×10^{-152}, OR=0.29, P-value=$1.0 \times 10^{-}$

[161] and OR=0.42, P-value=2.2×10^{-24}, respectively, in IAMDGC) and decreased levels of FHR-4 (β=-0.54, P-value=2.0×10^{-16}, β=-0.31, P-value=8.0×10^{-6} and β=-0.54, P-value=0.001, respectively, in our two-cohort meta-analysis), compared to reference H1:H1 genotype.

Using a sequential forward approach, we tested the association of the haplotypes formed by rs10922109 (1.1) and rs61818925 (1.6), the best two single-variant association signals with FHR-4 levels in our meta-analysis (Table 2). The most frequent haplotype CG ($H1^*$; controls 44%, cases 64% in IAMDGC) was used as reference. We observed three other haplotypes (H2*-H4*) carrying both distinct AMD lower risk (in IAMDGC; with similar OR estimates in our two-cohort meta-analysis) and distinct lowering effects on FHR-4 levels (Fig. 6A-C and Supplementary Data 11). Haplotype $H2^*$ (AT) showed the strongest association with FHR-4 levels (β=-0.52, P-value=2.4×10^{-58}) with a larger effect size and more significant P-value than any of the single-variant signals (Table 2). Haplotype $H4^*$ (AG) was the only haplotype also associated with FH levels (β=0.08, P-value=7.7×10^{-7}). Adding SNP rs570618 (1.2), the third meta-analysis single-variant association signal with FHR-4 levels (Table 2), to the inferred haplotypes did not significantly improve the dissection of the genetic effects on FHR-4 levels at the *CFH* locus (lowest P-value=2.0×10^{-53} at haplotype GAT, β=-0.50).

Discussion

Here we provide compelling evidence to show that AMD is associated with genetically-driven elevated circulating levels of FHR-4 and not associated with circulating FH levels. FHR-4 likely predisposes to disease by penetrating the ECM of the choriocapillaris and Bruch's membrane and acting locally by facilitating complement activation. FHL-1 is the complement regulator primarily responsible for protecting intercapillary septa ECM from complement activation,[6,15] but this protective function may be inhibited by FHR-4. FHR-4 accumulates in the intercapillary septa of the choriocapillaris, the ECM surrounding the fenestrated capillaries and a major site of AMD pathogenesis (Fig. 2A-E). *CFHR4* gene transcription was absent in the RPE and choroid, demonstrating that the systemic circulation is the source of FHR-4 in the eye. Deposition of C3b in the intercapillary septa will result in C3 convertase formation, complement activation and inflammation unless sufficiently regulated by FI-mediated C3b breakdown in the presence of FHL-1.[15] Based on our *in vitro* competition assays (Fig. 2J), we propose that in AMD, the accumulation of FHR-4 in the ECM out-competes FHL-1 for C3b binding, thereby preventing FI-mediated C3b breakdown and driving complement activation. FHR-4 bound to deposited C3b may also directly facilitate C3 convertase formation.[47,48] Excessive complement turnover, driven by FHR-4 accumulation, will continue to recruit and activate circulating immune cells,[49] another key feature of early AMD. Quite how complement over-activation leads to drusen formation remains unclear, although studies have demonstrated that a combination of both complement over activation and oxidative stress can result in lipid accumulation in RPE cells and Bruch's membrane.[50] Furthermore, non-canonical roles of complement have also been shown to influence the ability to clear apolipoproteins from RPE cells and Bruch's membranes in various animal models.[51]

Remarkably, the *CFH* locus was the only genome-wide significant locus in our GWAS meta-analysis of FHR-4 levels. The top signal is in tight LD with the strongest published AMD association signal at the *CFH* locus[5] (Fig. 4A, Supplementary Fig. 6A and Supplementary Data 3, Supplementary Data 4 and Supplementary Data 5). The triangular relationship between established susceptibility *CFH* locus variants, FHR-4 levels and AMD provides strong support for the association we observe between FHR-4 levels and increased AMD risk (Table 1, Fig. 1A and Supplementary Fig. 1A) to be causal. Our haplotype-based association analyses allowed the individual effects of FHR-4 levels, the *CFHR1-3* deletion and the Y402H variant of FH/FHL-1 to be dissected. Using the most frequent haplotype H1 (carrying the risk allele of Y402H) as reference, the two most protective haplotypes, H2 and H3, were associated with the lowest levels of FHR-4 (Fig. 5A-B and Supplementary Data 9). The H2 haplotype (carrying the FHR-4 lowering/AMD protective alleles A of rs10922109 (1.1) and T of rs61818925 (1.6)) does not contain the *CFHR1-3* deletion, suggesting that lower FHR-4 levels confer the disease-protective effect. Furthermore, the diplotype analysis demonstrates that the H1:H2 genotype is associated with disease protection relative to H1:H1, suggesting a dominant decreased disease risk effect of lower FHR-4 levels even in the presence of the Y402H risk variant on the other allele (Supplementary Data 10 and Supplementary Fig. 7). Finally, we showed that the two independently AMD-associated variants rs10922109 (1.1) and rs61818925 (1.6) are a minimal set of variants that explain the genetic effect on FHR-4 levels at the *CFH* locus (Fig. 6A-C).

FH levels were not different between cases and controls in our two independent cohorts (Fig. 1B and Supplementary Fig. 1B). Previous studies have measured systemic levels of FH in AMD and reported inconsistent results.[52-60] The sample size of our analysis (484 cases and 522 controls) exceeds all previous investigations. Our GWAS meta-analysis of FH levels reveals a

similar genetic structure to that previously reported,[52] with the top signal in high LD with variants that tag the common *CFHR1-3* deletion (Fig. 4B, Supplementary Fig. 6B, Supplementary Data 6, Supplementary Data 7 and Supplementary Data 8). The data also show that systemic FH and FHR-4 levels are dictated by a different genetic architecture (Supplementary Fig. 8). The top signal for FH levels, rs74696321 (β =-0.10, P-value=2.4×10^{-11}), is only among the genome-wide significant association tail for FHR-4 levels (653^{th} hit, P-value=7.4×10^{-9}) with opposite direction of allelic effect (β=0.23), while the top signal for FHR-4 levels, rs7535263 (β=-0.42, P-value=9.0×10^{-57}), tagging the top AMD-associated variant rs10922109, does not pass the genome-wide significance threshold in the GWAS meta-analysis of FH levels (β=0.03, P-value=0.005). It should be noted that the circulating levels of FHR-4 are clearly associated with AMD risk, but the molar ratios of FHR-4 and FH/FHL-1 in blood are not representative of the ratios of the accumulated proteins in the ECM of the choriocapillaris and Bruch's membrane. This can be attributed to the relatively large hydrodynamic size of FH compared to FHR-4 and FHL-1; we have previously shown that there is more FHL-1 in the tissue than FH, and that FH, unlike FHL-1, cannot diffuse across Bruch's membrane.[15,61] Furthermore, the absence of local FHR-4 expression in the eye emphasizes the relevance of systemic levels of this protein for its accumulation in the choriocapillaris, whereas FHL-1, and any FH that is present, may be derived locally or systemically.

Genetically driven variations in the levels and functions of alternative pathway complement proteins play a central role in AMD pathogenesis. Common and rare coding variants in *CFH* are important: the common Y402H variant and a majority of the rare variants in *CFH* identified to date (that generally result in a familial, early-onset condition) affect the function of both FHL-1 and FH, suggesting a particular role for FHL-1 in AMD pathogenesis[62,63]. However, there are rare variants affecting only FH, including the R1210C mutation, strongly associated with

early onset AMD, showing that full-length FH also has an important role[12]. In addition, mutations in *CFI* and common variants in *C3* and *CFB* modify AMD risk[5,64]. Therefore, it can be concluded that a balance between the actions of proteins that inhibit the alternative pathway (FH/FHL-1, FI) and those that activate the alternative pathway (C3, FB) influence AMD risk. Here we provide compelling data suggesting another regulator of the alternative pathway, FHR-4, is likely to have an important role in regulating this balance and thereby modifying AMD risk. This research implies that targeting FHR-4 may represent a future therapeutic avenue to explore in the treatment of AMD. Our demonstration that high systemic FHR-4 levels are associated with AMD risk makes the case for a therapy that lowers systemic FHR-4 levels; this could be achieved using antibodies or other agents that block or sequester the protein or by anti-sense targeting of hepatic FHR-4 synthesis. The efficacy of clinical trials evaluating FHR-4 inhibiting treatments could be enhanced by patient selection based on FHR-4 levels and the genetic markers identified here.

Methods

Study samples

The Cambridge AMD study is a case-control study with subjects recruited from the southeast and northwest of England between 2002-2006[65]. All affected subjects had choroidal neovascularization (CNV) and/or geographic atrophy (GA). Controls were spouses, partners or friends of index patients. Blood samples were obtained at the time of interview; EDTA and lithium-heparin plasma samples were used for DNA extraction and FHR-4/FH measurements respectively. The European Genetic Database (EUGENDA) created for clinical and molecular analysis of AMD comprises late AMD cases and controls recruited at Radboud University Medical Center, the Netherlands, and University of Cologne, Germany. Details on exclusion criteria and grading are provided in the Supplementary Methods. All participants provided written informed consent for clinical examination, epidemiological data collection, and blood sampling for biochemical and genetic analyses. Serum samples were used for FHR-4/FH measurements. Donor eye tissue was obtained from Manchester Eye Tissue Repository (ethically approved Research Tissue Bank, UK NHS Health Research Authority ref 15/NW/0932). The banked tissue was collected and stored within 48 hours of death; there was prior informed consent for research use. Human Tissue Act 2004 (UK) guidelines were followed. For all studies, ethical approval was obtained from either national or local ethics committees and adhered to the tenets of the Declaration of Helsinki.

Proteins and antibodies

Recombinant FHR-4 was made through the GenScript gene synthesis and protein expression service (Piscataway, NJ 08854 USA) using their baculovirus-insect cell expression system and

was based on the published sequence for the FHR-4B variant of the *CFHR* gene (UniProt identifier Q92496-3): the protein was designed to include a N-terminal 6x His tag and TEV cleavage site (Supplementary Fig. 9).

For the generation of specific FHR-4 monoclonal antibodies, mice were immunised subcutaneously (sc) with recombinant FHR-4 (~30µg/mouse) in complete Freund's adjuvant; boosted 4 and 6 weeks later with FHR-4 (dose as above) in incomplete Freund's adjuvant and test bled at 8 weeks. Mice with the highest titre in a screening assay on immobilized FHR-4 protein were selected and boosted intraperitoneally with FHR-4 (30µg in PBS), sacrificed 48 hours later and the spleen harvested aseptically. Spleen cells, obtained by perfusion with RPMI in a sterile cabinet, were fused with SP2 myeloma cells to generate hybridomas using standard protocols. Cells were plated at limiting dilution in 96-well plates and left undisturbed for 14 days. Supernatant (50µl) was removed from each well and screened for anti-FHR-4 titre as above. Positive clones were subjected to three rounds of re-cloning prior to expansion and large-scale culture. Antibodies were purified on protein G and tested in Western blotting against recombinant FHR-4 and human serum. Non-competitive pairs of antibodies were identified for ELISA development.

Recombinant FHL-1 was expressed in HEK293 cells as described previously[15]. Commercially available purified complement proteins used include C3b (VWR International, Lutterworth, UK, catalogue no. 204860), FH (Sigma-Aldrich, catalogue no. C5813), and FI (VWR International, catalogue no. 341280). Commercially available antibody against collagen IV was used (catalogue no: 600-401-106S, 2B Scientific Ltd., Oxford, UK).

FHR-4 and FH systemic level measurements

The levels of FHR-4 were measured using an optimised in-house sandwich ELISA. Nunc-Immuno™ MaxiSorp™ 96-well plates were coated with 50µl/well of monoclonal anti-FHR-4 antibody 4E9 at 5µg/ml (in 0.1M carbonate buffer pH9.6). After blocking in 2% BSA in PBS + 0.1%Tween-20 (PBST), plates were washed in PBST and a dilution series of purified FHR-4 protein diluted in 0.1% PBST added to wells in duplicate to generate a standard curve. Test samples were added (50µl/well) in duplicate at a 1:40 dilution to the remaining wells, and plates were incubated at 37°C for 1.5 hours. Plates were washed in PBST, 50µl/well of 1µg/ml of HRP-labelled anti-FHR-4 monoclonal antibody clone 17 was added and the plates were incubated for 1 hour at room temperature. After washing, 50µl/well of orthophenylenediamine (SIGMAFAST™ OPD, Sigma-Aldrich, UK) was added to develop the plates and the reaction was stopped after 5 minutes by adding an equal volume of 10% sulphuric acid. Absorbance was measured in a plate reader at 492 nm and protein concentrations were interpolated from the standard curve plotted using GraphPadPrism5.

FH levels were measured in a similar manner using monoclonal anti-FH antibody OX24 at 5µg/ml as capture, purified FH protein diluted in 0.1% PBST as standard, test samples at a 1:4000 dilution, HRP-labelled monoclonal anti-FH antibody 35H9 (1µg/ml) as detect, developed with OPD and read as above.

Immunohistochemistry

Human donor eye tissue sections were obtained from the Manchester Eye Tissue repository where 5 mm biopsies of the macula region from donor eyes were frozen in OCT and undergone cryo-sectioning (10 µm) that were subsequently stored at -80°C. Frozen tissue section slides were

stained for the presence of FHR-4, collagen IV or C3/C3b using methods described previously[15]. Briefly, tissue sections were incubated with chilled (-20 °C) histological grade acetone:methanol (1:1, v/v; Sigma-Aldrich) for 20 seconds before thorough washing with PBS. Tissue sections were blocked with 0.1% (w/v) BSA, 1% (v/v) goat serum, and 0.1% (v/v) Triton X-100 in PBS for 1 h at room temperature. After washing, tissue sections were incubated with Ab combinations of either 10 μg/ml of anti-FHR-4 monoclonal antibody (clone 150) mixed with either 1 μg/ml anti-Collagen IV rabbit polyclonal antibody, or 1 μg/ml anti-C3/C3b rabbit polyclonal antibody (catalogue no: 21337-1-AP, Proteintech Group, Inc, United States), for 16 h at 4 °C. Sections were washed and biotinylated anti-mouse IgG (Catalogue No. BA_9200, Vector laboratories, Inc) diluted 1:250 in PBS was applied for 1 hour to amplify the FHR-4 signal. Slides were subsequently washed and Alexa Fluor® 647 streptavidin (catalogue no: S32357, Invitrogen) diluted 1:250 in PBS and Alexa Fluor®488-conjugated goat anti-rabbit Ab (Invitrogen, USA) diluted 1:500 in PBS were added for 2 h at room temperature. After washing, DAPI was applied as a nuclear counterstain (at 0.3 mM for 5 min) prior to mounting with medium (Vectashield; H-1400, Vector Laboratories, Peterborough, UK) and application of a coverslip.

In the case of blank control sections, an identical protocol was followed but PBS replaced the primary antibody. To test antibody specificity in immunohistochemistry pre-adsorption experiments were performed whereby 10-fold molar excess of recombinant FHR-4 is premixed with the anti-FHR-4 mAb prior to application to the tissue sections (Supplementary Fig. 10). Further testing was performed by pre-absorbing with excess purified FHL-1 protein to ensure the anti-FHR-4 antibody did not cross-react (Supplementary Fig. 10). Furthermore, competition ELISAs were performed demonstrating the specificity of clone 150 for FHR-4 and not FH (Supplementary Fig. 11). In all cases images were collected on a Zeiss Axioimager.D2 upright

410 microscope using a 40x / 0.5 EC Plan-neofluar and 100x / 0.5 EC Plan-neofluar objective and
411 captured using a Coolsnap HQ2 camera (Photometrics) through Micromanager software v1.4.23.
412 Specific band pass filter sets for DAPI, FITC and Cy5 were used to prevent bleed through from
413 one channel to the next. Images were then processed and analysed using Fiji ImageJ
414 (http://imagej.net/Fiji/Download).

415

416 ***Surface plasmon resonance***

417 The binding of FHR-4 to immobilised C3b was measured by surface plasmon resonance (SPR)
418 using a Biacore 3000 (GE Healthcare). The sensor surfaces were prepared by immobilizing human
419 C3b onto the flow cells of a Biacore series S carboxymethylated dextran (CM5) sensor chip (GE
420 Healthcare) using standard amine coupling and included blank flow cells where no C3b protein
421 was present. Experiments were performed at 25°C and a flow rate of 15 µl/min in PBS with 0.05%
422 surfactant P20. FHR-4 was injected in triplicate at concentrations ranging from 1 to 100µg/ml.
423 Samples were injected for 150 seconds and dissociated for another 200 seconds; the chip was
424 regenerated with 1M NaCl for 1 min and re-equilibrated into PBS with 0.05% surfactant P20 prior
425 to the next injection. After subtraction of the blank cell value from each response value, association
426 and dissociation rate constants were determined by global data analysis. All curves were fitted
427 using a 1:1 Langmuir association/dissociation model (BIAevaluation 4.1; GE Healthcare).

428

429 ***Solid phase binding assays***

430 Purified C3b was adsorbed onto the wells of microtiter plates (Nunc Maxisorb, Kastrup, Denmark)
431 at 1µg/well in 100µl/well PBS for 16 h at room temperature. Plates were blocked for 90 minutes

at 37°C with 300µl/well 1% (w/v) BSA in standard assay buffer (SAB; 20mM HEPES, 130mM NaCl, 0.05% (v/v) Tween-20, pH 7.3). SAB was used for all subsequent incubations, dilutions and washes and all steps were performed at room temperature. A constant concentration of 100nM was made for either FH or FHL-1 in SAB and increasing concentrations of FHR-4 are used as competitor, up to 500nM. FH/FHR-4 and FHL-1/FHR-4 mixes were incubated with the immobilized C3b for 4 hours. After washing, bound FH or FHL-1 protein was detected by the addition of 100µl/well of 0.5µg/ml OX23 antibody and incubated for 30 minutes followed by washing and a 30-minute incubation in 100µl of a 1:1000 dilution of AP-conjugated anti- mouse IgG (Sigma-Aldrich). Plates were developed using 100µl/well of a 1mg/ml disodium *p*-nitrophenylphosphate solution (Sigma-Aldrich) in 0.05 M Tris-HCl, 0.1 M NaCl, pH 9.3. The absorbance values at 405 nm were determined after 10 minutes of development at room temperature and corrected against blank wells (*i.e.*, those with no immobilized C3b).

Fluid phase C3b breakdown assays

The fluid phase cofactor activity of FHL-1 was measured by incubating purified FHL-1, C3b and FI together in a total volume of 20µl PBS for 15 minutes at 37°C. For each reaction 2µg C3b and 0.04µg FI were used with varying concentrations of FHL-1 ranging from 0.015µg to 1µg per reaction. The assay was stopped by addition of 5µl 5× SDS reducing sample buffer and boiling for 10 minutes at 100°C. Samples were run on a 4-12% NuPAGE Bis Tris gel at 200V for 60 minutes in order to maximise the separation of the C3b breakdown product bands (Supplementary Fig. 4). Molecular weight markers used were Novex Sharp pre-stained protein standards (3.5-260kDa, Cat. No. LC5800, Life Technologies, Paisley, UK). The density of the 68kDa iC3b product band was measured using ImageJ64 (version 1.40g; rsb.info.nih.gov/ij) and used to track C3b breakdown

efficiency of the FHL-1 proteins. For FHR-4 inhibition assays, the amount of FHL-1 used in the reaction is fixed at 1μg and increasing amounts of FHR-4 were added to create up to a 5-fold molar excess of FHR-4 over FHL-1. Otherwise the reactions were performed under the same condition as previously. In all cases averaged data from three separate experiments were used.

Ussing chamber diffusion experiments

The macular region of enriched Bruch's membrane isolated from donor eyes was mounted in an Ussing chamber (Harvard Apparatus, Hamden, CT)[61]. Once mounted, the 5-mm-diameter macular area was the only barrier between two identical compartments (Supplementary Fig. 3). Both sides of Bruch's membrane were washed with 2 ml PBS for 5 min at room temperature. Fresh PBS was placed in both the sample and diffusate chambers. To the sample chamber, pure recombinant FHR-4, final concentration of 100μg/ml, was added and the Ussing chamber was left at room temperature for 24 hours with gentle stirring in each compartment to avoid generating gradients of diffusing protein. Samples from each chamber were analyzed on 4-12% NuPAGE Bis-Tris gels, run at 200V for 60 minutes. Either 20μl samples straight from each chamber were mixed with 5μl 5x SDS loading buffer and run or 100μl samples were taken and concentrated using StrataClean beads (hydroxylated silica; Agilent Technologies, Cheadle, U.K) for 5 minutes at room temperature before centrifugation. Beads were then re-suspended in 20μl neat 5x SDS loading buffer and loaded directly to the gel. Gels were stained with Instant Blue stain (Expedeon, Harston, U.K.) for 60 min at room temperature, before washing and storage in MiliQ water. Molecular weight markers used were Blue Prestained Protein Standards, Broad Range (11-190kDa, New England BioLabs, Hitchin, UK, catalogue no. P7706S). Diffusion experiments were performed on three separate donor BrM.

478

479 ***Genotype data and association analysis***

480 All individuals included in this study had been previously genotyped with a custom-
481 modified Illumina HumanCoreExome array at the Center for Inherited Disease Research (CIDR)
482 and analysed within the IAMDGC GWAS (43,566 subjects; 16,144 advanced AMD cases and
483 17,832 controls of European ancestry)[5]. Quality control and genotype imputation using the 1000
484 Genomes Project[66] reference panel were performed by the IAMDGC as described previously[5]. A
485 total of 9,618,989 quality-controlled common (Minor Allele Frequency, MAF ≥ 1%) variants
486 (289,971 genotyped; 9,329,018 imputed) were available for the 1,006 individuals included in this
487 study. Phased genotype data as inferred within the IAMDGC study[5] were also available and used
488 in the haplotype-based association analyses. All statistical association analyses were conducted on
489 each cohort separately (Cambridge and EUGENDA), and combined as 2-stage, fixed-effects meta-
490 analyses of the available individual participant data from the two cohorts. Heterogeneity across
491 studies was assessed using the I^2 statistic. FHR-4 and FH levels were natural logarithmically
492 transformed to ensure normality of the distribution when using linear regression models. We
493 assessed the association of late AMD with natural logarithmically transformed FHR-4/FH levels
494 via Wald tests using linear regression models adjusted for sex, age, batch effects and the first two
495 genetic principal components (as estimated within the IAMDGC study[5]). We also reported the
496 association of FHR-4/FH levels with late AMD via OR expressed as per standard deviation (SD)
497 change of log-levels using logistic regression models adjusted for sex, age, batch effects and the
498 first two genetic principal components. We assessed the association of the 8 independently AMD-
499 associated variants at the *CFH* locus reported by the IAMDGC study[5] (i.e., rs10922109 [1.1],
500 rs570618 [1.2], rs121913059 [1.3], rs148553336 [1.4], rs187328863 [1.5], rs61818925 [1.6],
501 rs35292876 [1.7], rs191281603 [1.8]; Supplementary Data 1) with natural logarithmically

transformed FHR-4/FH levels via Wald tests on the variant genotypes coded as 0, 1 and 2 according to the number of minor alleles for the directly typed variants or allele dosages for the imputed variants, using linear regression models adjusted for sex, age, batch effects and the first two genetic principal components in controls and in all samples further adjusting for AMD status. The single-SNP association with AMD was assessed with ORs expressed as per 1 minor allele, using logistic regression models adjusted for the first two genetic principal components. Finally, we extracted the best-guess (i.e., most likely) haplotypes formed by the AMD-associated variants at the *CFH* locus considered in our analysis and additionally included rs6677604 as proxy for the AMD-protective *CFHR1-3* deletion[29], using the phased genotype data produced within the IAMDGC study[5]. The association of the observed haplotypes with AMD was assessed using logistic regression models adjusted for the first two genetic principal components, and with FHR-4/FH levels using linear regression models adjusted for AMD status, sex, age, batch effects, and the first two genetic principal components. The haplotype-based association with AMD was also performed on the whole IAMDGC primary analysis dataset of 16,144 patients with advanced AMD and 17,832 control subjects of European ancestry using logistic regression models adjusted for whole-genome amplification and the first two genetic principal components as per the IAMDGC study[5]. All the statistical analyses above were conducted using Stata software, version 13.1 (StataCorp); *tobit* command was used for censored regression models to take into account any 'below of detection' FHR-4 levels (n=16 data points equal to baseline 0.504116; with virtually identical results as per *regress* command for linear regression models), *ipdmetan* and *mvmeta* commands were used for conducting meta-analyses of individual participant data.

We also carried out GWASs of natural logarithmically transformed FHR-4 and FH levels in controls from each cohort (Cambridge and EUGENDA) using linear regression models adjusted

for sex, age, batch effects and the first two genetic principal components, and in all samples further adjusting for AMD status. The GWASs were carried out using EPACTS software (http://genome.sph.umich.edu/wiki/EPACTS) and Wald tests were performed on the variant genotypes coded as 0, 1 and 2 according to the number of minor alleles for the directly typed variants or allele dosages for the imputed variants. Genomic control correction[67] was applied if lambda was greater than 1. Effect size estimates and standard errors of single variants seen in both cohorts were subsequently combined in a fixed-effect meta-analysis using METAL[68]. This meta-analysis had a statistical power of over 80% to detect associations of genetic variants with a MAF ≥ 1% explaining ≥ 3.9% of the variance in FHR-4 levels (Genetic Power Calculator: http://zzz.bwh.harvard.edu/gpc/). Manhattan and Q-Q plots were generated using the *qqman* R package (version 0.1.2). Regional plots of association were generated using LocusZoom (version v0.4.8)[69]. Finally, linkage disequilibrium measures (R^2 and D') were calculated using LDlink (https://ldlink.nci.nih.gov/), based on the European (EUR) population genotype data originates from Phase 3 (Version 5) of the 1000 Genomes Project[66].

Data availability

The summary statistics for the GWAS meta-analyses of FHR-4 and FH levels are available through the GWAS Catalog, https://www.ebi.ac.uk/gwas/, [accession codes will be available before publication].

The Gene Expression Omnibus datasets used for the gene expression analyses are available at: https://www.ncbi.nlm.nih.gov/geo/query/acc.cgi?acc=GSE18811, dataset name: GSE18811; https://www.ncbi.nlm.nih.gov/geo/query/acc.cgi?acc=GSE41102, dataset name: GSE41102; https://www.ncbi.nlm.nih.gov/geo/query/acc.cgi?acc=GSE50195, dataset name: GSE50195; https://www.ncbi.nlm.nih.gov/geo/query/acc.cgi?acc=GSE94437, dataset name: GSE94437; https://www.ncbi.nlm.nih.gov/geo/query/acc.cgi?acc=GSE99248, dataset name: GSE:99248.

The Genotype-Tissue Expression (GTEx) Project datasets used for the gene expression analyses were obtained from the GTEx Portal, https://gtexportal.org/home/multiGeneQueryPage (4/4/2018), dataset dbGaP accession number phs000424.v8.p2; the GTEx Project was supported by the Common Fund of the Office of the Director of the National Institutes of Health, and by NCI, NHGRI, NHLBI, NIDA, NIMH, and NINDS.

The source data underlying Figs. 1, 2B-I, 3B, 4, 5A, 6A-B and Supplementary Figs. 2A, 5, 6, 7A-D, 8, 10A, 11 are provided as a Source Data file.

All other datasets and reagents generated/used in the current study are available from the corresponding authors upon reasonable request.

References

1. Wong, W.L., *et al.* Global prevalence of age-related macular degeneration and disease burden projection for 2020 and 2040: a systematic review and meta-analysis. *Lancet Glob Health* **2**, e106-116 (2014).
2. Curcio, C.A. Soft Drusen in Age-Related Macular Degeneration: Biology and Targeting Via the Oil Spill Strategies. *Invest Ophthalmol Vis Sci* **59**, AMD160-AMD181 (2018).
3. Crabb, J.W. The proteomics of drusen. *Cold Spring Harb Perspect Med* **4**, a017194 (2014).
4. Ferris, F.L., 3rd, *et al.* Clinical classification of age-related macular degeneration. *Ophthalmology* **120**, 844-851 (2013).
5. Fritsche, L.G., *et al.* A large genome-wide association study of age-related macular degeneration highlights contributions of rare and common variants. *Nat Genet* **48**, 134-143 (2016).
6. McHarg, S., Clark, S.J., Day, A.J. & Bishop, P.N. Age-related macular degeneration and the role of the complement system. *Mol Immunol* **67**, 43-50 (2015).
7. Schramm, E.C., *et al.* Genetic variants in the complement system predisposing to age-related macular degeneration: a review. *Mol Immunol* **61**, 118-125 (2014).
8. Edwards, A.O., *et al.* Complement factor H polymorphism and age-related macular degeneration. *Science* **308**, 421-424 (2005).
9. Hageman, G.S., *et al.* A common haplotype in the complement regulatory gene factor H (HF1/CFH) predisposes individuals to age-related macular degeneration. *Proc Natl Acad Sci U S A* **102**, 7227-7232 (2005).
10. Haines, J.L., *et al.* Complement factor H variant increases the risk of age-related macular degeneration. *Science* **308**, 419-421 (2005).
11. Klein, R.J., *et al.* Complement factor H polymorphism in age-related macular degeneration. *Science* **308**, 385-389 (2005).
12. Raychaudhuri, S., *et al.* A rare penetrant mutation in CFH confers high risk of age-related macular degeneration. *Nat Genet* **43**, 1232-1236 (2011).
13. Fontaine, M., *et al.* Truncated forms of human complement factor H. *Biochem J* **258**, 927-930 (1989).
14. Ripoche, J., Day, A.J., Harris, T.J. & Sim, R.B. The complete amino acid sequence of human complement factor H. *Biochem J* **249**, 593-602 (1988).
15. Clark, S.J., *et al.* Identification of Factor H-like Protein 1 as the Predominant Complement Regulator in Bruch's Membrane: Implications for Age-Related Macular Degeneration. *J Immunol* **193**, 4962-4970 (2014).
16. de Jorge, E.G., *et al.* Dimerization of complement factor H-related proteins modulates complement activation in vivo. *P Natl Acad Sci USA* **110**, 4685-4690 (2013).
17. Clark, S.J. & Bishop, P.N. Role of Factor H and Related Proteins in Regulating Complement Activation in the Macula, and Relevance to Age-Related Macular Degeneration. *J Clin Med* **4**, 18-31 (2015).
18. Triebwasser, M.P., *et al.* Rare Variants in the Functional Domains of Complement Factor H Are Associated With Age-Related Macular Degeneration. *Invest Ophthalmol Vis Sci* **56**, 6873-6878 (2015).
19. Geerlings, M.J., *et al.* The Functional Effect of Rare Variants in Complement Genes on C3b Degradation in Patients With Age-Related Macular Degeneration. *JAMA Ophthalmol* **135**, 39-46 (2017).
20. Hoffman, J.D., *et al.* Rare complement factor H variant associated with age-related macular degeneration in the Amish. *Invest Ophthalmol Vis Sci* **55**, 4455-4460 (2014).

21. Yu, Y.*, et al.* Whole-exome sequencing identifies rare, functional CFH variants in families with macular degeneration. *Hum Mol Genet* **23**, 5283-5293 (2014).
22. Geerlings, M.J., de Jong, E.K. & den Hollander, A.I. The complement system in age-related macular degeneration: A review of rare genetic variants and implications for personalized treatment. *Mol Immunol* **84**, 65-76 (2017).
23. Calippe, B.*, et al.* Complement Factor H Inhibits CD47-Mediated Resolution of Inflammation. *Immunity* **46**, 261-272 (2017).
24. Laine, M.*, et al.* Y402H polymorphism of complement factor H affects binding affinity to C-reactive protein. *J Immunol* **178**, 3831-3836 (2007).
25. Weismann, D.*, et al.* Complement factor H binds malondialdehyde epitopes and protects from oxidative stress. *Nature* **478**, 76-81 (2011).
26. Clark, S.J.*, et al.* Impaired Binding of the Amd-Associated Complement Factor H 402h Allotype to Bruch's Membrane in Human Retina. *Investigative Ophthalmology & Visual Science* **51**, 400 (2010).
27. Fritsche, L.G.*, et al.* An imbalance of human complement regulatory proteins CFHR1, CFHR3 and factor H influences risk for age-related macular degeneration (AMD). *Human Molecular Genetics* **19**, 4694-4704 (2010).
28. Hageman, G.S.*, et al.* Extended haplotypes in the complement factor H (CFH) and CFH-related (CFHR) family of genes protect against age-related macular degeneration: characterization, ethnic distribution and evolutionary implications. *Ann Med* **38**, 592-604 (2006).
29. Hughes, A.E.*, et al.* A common CFH haplotype, with deletion of CFHR1 and CFHR3, is associated with lower risk of age-related macular degeneration. *Nature Genetics* **38**, 1173-1177 (2006).
30. Raychaudhuri, S.*, et al.* Associations of CFHR1–CFHR3 deletion and a CFH SNP to age-related macular degeneration are not independent. *Nature Genetics* **42**, 553 (2010).
31. Spencer, K.L.*, et al.* Deletion of CFHR3 and CFHR1 genes in age-related macular degeneration. *Human Molecular Genetics* **17**, 971-977 (2008).
32. Kubista, K.E.*, et al.* Copy number variation in the complement factor H-related genes and age-related macular degeneration. *Mol Vis* **17**, 2080-2092 (2011).
33. Cantsilieris, S.*, et al.* Recurrent structural variation, clustered sites of selection, and disease risk for the complement factor H (CFH) gene family. *Proc Natl Acad Sci U S A* **115**, E4433-E4442 (2018).
34. Sivakumaran, T.A.*, et al.* A 32 kb critical region excluding Y402H in CFH mediates risk for age-related macular degeneration. *Plos One* **6**, e25598 (2011).
35. Chirco, K.R.*, et al.* Evaluation of serum and ocular levels of membrane attack complex and C-reactive protein in CFH-genotyped human donors. *Eye* **32**, 1740-1742 (2018).
36. Keenan, T.D.L.*, et al.* Assessment of Proteins Associated With Complement Activation and Inflammation in Maculae of Human Donors Homozygous Risk at Chromosome 1 CFH-to-F13B. *Investigative Ophthalmology & Visual Science* **56**, 4870-4879 (2015).
37. Mullins, R.F.*, et al.* The Membrane Attack Complex in Aging Human Choriocapillaris Relationship to Macular Degeneration and Choroidal Thinning. *Am J Pathol* **184**, 3142-3153 (2014).
38. Whitmore, S.S.*, et al.* Complement activation and choriocapillaris loss in early AMD: Implications for pathophysiology and therapy. *Prog Retin Eye Res* **45**, 1-29 (2015).
39. Lores-Motta, L.*, et al.* Genome-Wide Association Study Reveals Variants in CFH and CFHR4 Associated with Systemic Complement Activation: Implications in Age-Related Macular Degeneration. *Ophthalmology* (2018).
40. Strunz, T.*, et al.* A mega-analysis of expression quantitative trait loci (eQTL) provides insight into the regulatory architecture of gene expression variation in liver. *Scientific Reports* **8**(2018).

41. Strunnikova, N.V., *et al.* Transcriptome analysis and molecular signature of human retinal pigment epithelium. *Human Molecular Genetics* **19**, 2468-2486 (2010).
42. Wagner, A.H., *et al.* Exon-level expression profiling of ocular tissues. *Exp Eye Res* **111**, 105-111 (2013).
43. Whitmore, S.S., *et al.* Altered gene expression in dry age-related macular degeneration suggests early loss of choroidal endothelial cells. *Molecular Vision* **19**, 2274-2297 (2013).
44. Li, M.Y., *et al.* Comprehensive analysis of gene expression in human retina and supporting tissues. *Human Molecular Genetics* **23**, 4001-4014 (2014).
45. Kim, E.J., *et al.* Complete Transcriptome Profiling of Normal and Age-Related Macular Degeneration Eye Tissues Reveals Dysregulation of Anti-Sense Transcription. *Scientific Reports* **8**, 3040 (2018).
46. GTEx Consortium. Human genomics. The Genotype-Tissue Expression (GTEx) pilot analysis: multitissue gene regulation in humans. *Science* **348**, 648-660 (2015).
47. Hebecker, M. & Józsi, M. Factor H-related Protein 4 Activates Complement by Serving as a Platform for the Assembly of Alternative Pathway C3 Convertase via Its Interaction with C3b Protein. *Journal of Biological Chemistry* **287**, 19528-19536 (2012).
48. Hellwage, J., *et al.* Functional properties of complement factor H-related proteins FHR-3 and FHR-4: binding to the C3d region of C3b and differential regulation by heparin. *FEBS Lett* **462**, 345-352 (1999).
49. Clark, S.J. & Bishop, P.N. The eye as a complement dysregulation hotspot. *Semin Immunopathol* **40**, 65-74 (2018).
50. Kunchithapautham, K., Atkinson, C. & Rohrer, B. Smoke Exposure Causes Endoplasmic Reticulum Stress and Lipid Accumulation in Retinal Pigment Epithelium through Oxidative Stress and Complement Activation. *Journal of Biological Chemistry* **289**, 14534-14546 (2014).
51. Toomey, C.B., Kelly, U., Saban, D.R. & Rickman, C.B. Regulation of age-related macular degeneration-like pathology by complement factor H. *P Natl Acad Sci USA* **112**, E3040-E3049 (2015).
52. Ansari, M., *et al.* Genetic influences on plasma CFH and CFHR1 concentrations and their role in susceptibility to age-related macular degeneration. *Human Molecular Genetics* **22**, 4857-4869 (2013).
53. Guymer, R., *et al.* Plasma levels of amyloid beta and other proinflammatory mediators in patients with age-related macular degeneration. *Graef Arch Clin Exp* **253**, 1347-1354 (2015).
54. Hakobyan, S., *et al.* Measurement of factor H variants in plasma using variant-specific monoclonal antibodies: Application to assessing risk of age-related macular degeneration. *Investigative Ophthalmology & Visual Science* **49**, 1983-1990 (2008).
55. Reynolds, R., *et al.* Plasma Complement Components and Activation Fragments: Associations with Age-Related Macular Degeneration Genotypes and Phenotypes. *Investigative Ophthalmology & Visual Science* **50**, 5818-5827 (2009).
56. Scholl, H.P.N., *et al.* Systemic Complement Activation in Age-Related Macular Degeneration. *Plos One* **3**(2008).
57. Sharma, N.K., *et al.* Association between CFH Y402H Polymorphism and Age Related Macular Degeneration in North Indian Cohort. *Plos One* **8**(2013).
58. Sharma, N.K., *et al.* Predictive Model for Earlier Diagnosis of Suspected Age-Related Macular Degeneration Patients. *DNA Cell Biol* **32**, 549-555 (2013).
59. Silva, A.S., *et al.* Plasma levels of complement proteins from the alternative pathway in patients with age-related macular degeneration are independent of Complement Factor H Tyr^{402}His polymorphism. *Mol Vis* **18**, 2288-2299 (2012).

60. Smailhodzic, D.*, et al.* Risk alleles in CFH and ARMS2 are independently associated with systemic complement activation in age-related macular degeneration. *Ophthalmology* **119**, 339-346 (2012).
61. Clark, S.J., McHarg, S., Tilakaratna, V., Brace, N. & Bishop, P.N. Bruch's Membrane Compartmentalizes Complement Regulation in the Eye with Implications for Therapeutic Design in Age-Related Macular Degeneration. *Frontiers in Immunology* **8**(2017).
62. Taylor, R.L.*, et al.* Loss-of-Function Mutations in the CFH Gene Affecting Alternatively Encoded Factor H-like 1 Protein Cause Dominant Early-Onset Macular Drusen. *Ophthalmology* (2019).
63. Wagner, E.K.*, et al.* Mapping rare, deleterious mutations in Factor H: Association with early onset, drusen burden, and lower antigenic levels in familial AMD. *Sci Rep* **6**, 31531 (2016).
64. Kavanagh, D.*, et al.* Rare genetic variants in the CFI gene are associated with advanced age-related macular degeneration and commonly result in reduced serum factor I levels. *Hum Mol Genet* **24**, 3861-3870 (2015).
65. Yates, J.R.W.*, et al.* Complement C3 variant and the risk of age-related macular degeneration. *New Engl J Med* **357**, 553-561 (2007).
66. Abecasis, G.R.*, et al.* An integrated map of genetic variation from 1,092 human genomes. *Nature* **491**, 56-65 (2012).
67. Devlin, B. & Roeder, K. Genomic control for association studies. *Biometrics* **55**, 997-1004 (1999).
68. Willer, C.J., Li, Y. & Abecasis, G.R. METAL: fast and efficient meta-analysis of genomewide association scans. *Bioinformatics* **26**, 2190-2191 (2010).
69. Pruim, R.J.*, et al.* LocusZoom: regional visualization of genome-wide association scan results. *Bioinformatics* **26**, 2336-2337 (2010).

End notes

Acknowledgments

We are grateful to all the subjects who kindly participated in this research. For the Cambridge AMD Study (UK Medical Research Council (MRC) grant G0000067 to J.R.W.Y. and A.T.M.), we gratefully acknowledge help with patient recruitment from members of the Genetic Factors in AMD Study Group (P. Black, Z. Butt, V. Chong, C. Edelsten, A. Fitt, D.W. Flanagan, A. Glenn, S.P. Harding, C. Jakeman, C. Jones, R.J. Lamb, V. Moffatt, C.M. Moorman, R.J. Pushpanathan, E. Redmond, T. Rimmer and D.A. Thurlby); we thank Jane Khan and Humma Shahid for carrying out the clinical evaluation and sampling of subjects and Tunde Peto and colleagues at the Reading Centre, Moorfields Eye Hospital, London, for grading the fundus photographs. EUGENDA was funded by grants from the Oogfonds, MaculaFonds, Landelijke Stiching voor Blinden en Slechtzienden, Stichting Blindenhulp, Stichting A.F. Deutman Oogheelkunde Researchfonds, the Netherlands Organization for Scientific Research (Vidi Innovational Research Award 016.096.309), and the European Research Council under the European Union's Seventh Framework Programme (FP/2007-2013) (ERC Grant Agreement n. 310644 MACULA). We wish to thank the Manchester Eye Tissue Repository for supplying human macula tissue, and their funding from the Macular Society UK (12928). We also thank the International AMD Genomics Consortium (IAMDGC, http://eaglep.case.edu/iamdgc_web/) for providing the genotype data. The Cambridge and EUGENDA samples were genotyped as part of the IAMDGC exome-chip project supported by CIDR (contract number HHSN268201200008I) and funded by EY022310 (to Jonathan L. Haines, Case Western Reserve University, Cleveland) and 1 × 01HG006934-01 (to Gonçalo R. Abecasis, University of Michigan, Department of Biostatistics). We wish to thank Lars Fritsche for providing *CFH* locus phased genotype data. Other funding sources are as follows:

S.J.C./V.T., an MRC fellowship (MR/K024418/1); S.M., Fight for Sight UK research grant (1517/1518); B.P.M./D.F. supported by a Programme Grant from the MRC-supported UK Dementia Research Institute; V.C. was primarily funded by the Department of Health's NIHR Biomedical Research Centre for Ophthalmology at Moorfields Eye Hospital and UCL Institute of Ophthalmology, and an MRC research grant (MR/P025838/1).

The funding bodies had no role in the design of the study and collection, analysis, and interpretation of data and in writing the manuscript.

Author contributions

V.C. and **L.L.M**. performed the statistical association analyses and primarily wrote the manuscript. **F.H**. performed IHC for FHR-4, collagen IV and C3b on human macular tissue sections. **D.F.** performed FH and FHR-4 blood level analysis in both Cambridge and EUGENDA cohorts. **V.T.** made recombinant FHL-1 used in biochemical experiments and FHR-4 used to generate anti-FHR-4 antibody. **S.M**. collected and processed human eye tissue for the study. **N.B**. re-analyzed gene expression data from the public data repository's Gene Expression Omnibus and Expression Atlas. **İ.E.A.** helped with the GWAS meta-analyses of FHR-4 and FH levels. **A.T.M**. and **J.R.W.Y**. are principal investigators for the Cambridge AMD study, collected patient blood samples and clinical and genetic data. **C.H.**, **S.F.**, **E.dJ**. and **A.dH**. collected patient blood samples and are custodians of the EUGENDA sample cohort. **B.P.M**. generated anti-FHR-4 monoclonal antibodies, designed and optimised the FH and FHR-4 specific ELISA, and contributed to the primary writing of the manuscript. **P.N.B** contributed to the design of experiments, to collection of Cambridge AMD study samples, writing of the manuscript and supervised IHC experiments. **S.J.C**. coordinated the project, performed biochemical analysis including binding, competition and

C3b breakdown assays with FHR-4, designed IHC experiments, and contributed to the primary writing of the manuscript.

All authors contributed to data interpretation and the final version of the manuscript text.

Competing interests

The authors declare no competing interests.

Figure legends

Figure 1. Systemic FHR-4 levels are elevated in AMD patients.

Panel A shows box plots of FHR-4 levels measured in two separate AMD cohorts: Cambridge (plasma from 214 controls and 304 late AMD cases) and EUGENDA (serum from 308 controls and 180 late AMD cases). AMD patients show statistically significant elevated FHR-4 levels compared to controls. Geometric mean FHR-4 levels were: Cambridge, 5.5µg/ml in controls *vs* 6.6µg/ml in cases; EUGENDA, 6.0µg/ml in controls *vs* 7.2µg/ml in cases. These differences remained significant after adjustment for sex, age and batch effects (P-value=0.017 and P-value=$9.6x10^{-5}$ for Cambridge and EUGENDA, respectively). Panel B shows box plots of FH levels measured in the same samples, where no statistically significant difference between cases and controls was observed: Cambridge, 349.0µg/ml in controls *vs* 348.6µg/ml in cases; EUGENDA, 304.7µg/ml in controls *vs* 308.7µg/ml in cases. Source data are provided as a Source Data file.

Figure 2. Accumulation of FHR-4 in the choriocapillaris inhibits C3b breakdown.

Panel A shows a schematic diagram illustrating anatomical structures in the macula including the retinal pigment epithelium (RPE), the underlying Bruch's membrane (BrM) and the intercapillary septa within the choriocapillaris; basement membranes are represented as black lines. Drusen, hallmark lesions of early AMD, form within BrM underneath the RPE basement membrane. Panels B-C: immunohistochemistry showing the localisation of FHR-4 (yellow) predominantly in the intercapillary septa: weak labeling is also seen within BrM. Collagen IV staining is used to delineate basement membranes which define the inner and outer borders of BrM (red), DAPI

799 labeling is in blue. FHR-4 is also localized in drusen (panel D); the RPE is absent from these tissue
800 sections. Panel E: both FHR-4 and C3/C3b localize in the intercapillary septa of the
801 choriocapillaris (white arrow): scale bars 20μm. SPR analysis showing the binding of FHR-4 to
802 immobilized C3b (panel F). Solid phase binding assays demonstrate that FHR-4 can compete off
803 fluid phase FH or FHL-1 binding to immobilized C3b (panel G). Measurement of FHL-1 mediated
804 breakdown of C3b by factor I (panel H); in the presence of fixed concentrations of C3b and factor
805 I, increasing concentrations of FHL-1 result in increased breakdown of the C3b α-chain (see
806 Supplementary Fig. 4 for full gel image). Panel I: optimal C3b breakdown conditions from panel
807 H are repeated but now include increased concentrations of fluid-phase FHR-4, where an inhibition
808 of FHL-1/FI-mediated C3b α-chain breakdown is observed (see Supplementary Fig. 4 for full gel
809 image). Panel J: FHR-4 prevents FHL-1 acting as a cofactor for factor I, this results in the
810 formation of a C3 convertase and the activation of the amplification loop of complement and
811 subsequent inflammation. Source data are provided as a Source Data file.
812
813 **Figure 3. Four established AMD risk variants at the *CFH* locus are strongly associated with**
814 **FHR-4 levels.**
815 Schematic diagram of chromosome 1 showing the genes in the *CFH* locus and the genomic
816 location of the 8 established AMD risk variants from the large IAMDGC GWAS of AMD[5] and
817 rs6677604, a proxy for the previously reported AMD protective *CFHR1-3* deletion[29] (panel A).
818 Variant annotations are in red or blue depending on whether the corresponding minor allele is
819 AMD deleterious or protective. The rare missense variant rs121913059 (1.3; R1210C) was only
820 present heterozygously in a case individual from the Cambridge cohort, and therefore was not
821 included in the genetic association analyses with the FHR-4/FH levels. Panel B shows box plots

of FHR-4 levels by AMD status and SNP genotype for the four variants that showed significant associations (after Bonferroni correction) with FHR-4 levels (Table 2), in the Cambridge and EUGENDA cohorts combined. Source data are provided as a Source Data file.

Figure 4. GWAS meta-analysis of FHR-4 levels reveals a strong genome-wide significant signal spanning the *CFH* locus.

Each panel shows a Manhattan plot, a regional plot (upper left-hand side) and a quantile-quantile (QQ) plot (upper right-hand side) for the results of the GWAS meta-analysis of FHR-4 levels (panel A) and FH levels (panel B). Manhattan plots illustrate P-values for each single variant tested for association with log(levels). Observed $-\log_{10}$(P-values) are plotted against the genomic position of each variant on chromosomes 1–22 plus the X chromosome. The horizontal red line indicates the threshold considered for genome-wide significance (P-value $\leq 5 \times 10^{-8}$). Regional plots show the only genome-wide association signal observed, i.e., at the *CFH* locus (on chromosome 1q31.3). The most associated variant is denoted by a purple circle and is labelled by its rsID. The other surrounding variants are shown by circles coloured to reflect the extent of LD with the most associated variant (based on 1000 Genomes data, November 2014). A diagram of the genes within the relevant regions is depicted below each plot. Physical positions are based on NCBI RefSeq hg19 human genome reference assembly. QQ plots compare the distribution of the observed test statistics with its expected distribution under the null hypothesis of no association. A marked departure from the null hypothesis (red line) is seen in the meta-analysis of FHR4 levels. Genomic inflation values (λ) were equal to 1.008 and 1.005 from the GWASs of FHR-4 levels and 1.002 and 1.014 from the GWASs of FH levels, in the Cambridge and EUGENDA studies, respectively.

Figure 5. Haplotype association analysis using established AMD risk variants at the *CFH* locus identifies haplotypes strongly associated with both AMD and FHR-4 levels.

Panel A illustrates the association of the observed common 9 haplotypes formed by the 7 AMD-associated *CFH* locus variants considered in our genetic association analyses and rs6677604 (overall haplotype frequency ≥ 1% in the Cambridge and EUGENDA cohorts combined, accounting for 98.5% of 2,012 chromosomes) with AMD and with FHR-4/FH levels. Details of the alleles forming the haplotypes together with the frequency distribution in the two cohorts combined, and as estimated in the whole IAMDGC dataset[5] (16,144 patients with advanced AMD and 17,832 control subjects of European ancestry), are shown in panel B: haplotype CTTGCCGC (H1) that carries the AMD increasing-risk allele T of the proxy for Y402H (1.2) is used as reference (colored in red); alleles that are different from the reference are colored in blue; the direction of association with AMD for the minor allele of each single variant as estimated in the IAMDGC study[5] is indicated in parentheses. Four association plots are displayed in panel A: the first two (*top*) plots show the OR (with CI) estimates for the *CFH* haplotype association with AMD in the IAMDGC dataset and our two-cohort meta-analysis, respectively; the third and fourth (*bottom*) plots show the Beta (with CI) estimates for the *CFH* haplotype association with FHR-4 and FH levels, respectively, in our two-cohort meta-analysis; haplotype H1 is used as reference. The estimates shown in each plot are labelled further to indicate the presence of alleles that differ from the referent haplotype; those alleles are indicated with the IAMDGC association signal numbers of the corresponding variants (1.1, 1.5-1.7), in red to indicate that the allele different from the reference is AMD risk-increasing, in blue if protective; the Y402H label is blue to indicate the presence of the protective allele G of variant 1.2, red for the AMD risk-increasing allele T; finally,

the label DEL indicates the presence of the protective allele A of the proxy for the *CFHR1-3* deletion (rs6677604). See Supplementary Data 9 for full details of the haplotype association estimates. Source data are provided as a Source Data file.

Figure 6. The two independently AMD-associated variants rs10922109 (1.1) and rs61818925 (1.6) are a minimal set of variants that explain the genetic effect on FHR-4 levels at the *CFH* locus in the Cambridge and EUGENDA meta-analysis.

Panel A illustrates the association of the observed 4 haplotypes formed by the 2 independently AMD-associated variants rs10922109 (1.1) and rs61818925 (1.6) at the *CFH* locus with AMD and with FHR-4/FH levels. Variants 1.1 and 1.6 represent the best two single-variant association signals with FHR-4 levels in the Cambridge and EUGENDA meta-analysis (Table 2). Details of the alleles forming the haplotypes together with the frequency distribution in the two cohorts combined (484 patients with advanced AMD and 522 controls) and as estimated in the whole IAMDGC dataset[5] (16,144 patients with advanced AMD and 17,832 control subjects of European ancestry) are shown in panel C: most common haplotype CG ($H1^{*}$) is used as reference (colored in red); alleles that are different from the reference are colored in blue; the direction of association with AMD for the minor allele of each single variant as estimated in the IAMDGC study[5] is indicated in parentheses. Four association plots are displayed in panel A: the first two (*top*) plots show the OR (with CI) estimates for the *CFH* haplotype association with AMD in the IAMDGC dataset and our two-cohort meta-analysis, respectively; the third and fourth (*bottom*) plots show the Beta (with CI) estimates for the *CFH* haplotype association with FHR-4 and FH levels, respectively, in our two-cohort meta-analysis; haplotype $H1^{*}$ is used as reference. The estimates shown in each plot are labelled further to indicate the presence of alleles that differ from the

referent haplotype; those alleles are indicated with the IAMDGC association signal numbers of the corresponding variants (1.1 and 1.6), in blue to indicate that the allele different from the reference is AMD protective. See Supplementary Data 11 for full details of the rs10922109-rs61818925 haplotype association estimates. Finally, panel B shows box plots of FHR-4 levels (*top*) and FH levels (*bottom*) by rs10922109-rs61818925 haplotype for each study cohort (Cambridge and EUGENDA). Source data are provided as a Source Data file.

Table 1. Demographics of study cohorts and association analyses between AMD and systemic FHR-4/FH levels

	Cambridge		EUGENDA		
	Controls	**Cases**	**Controls**	**Cases**	
	214	304	308	180	
	75.2 (8.0)	74.1 (8.3)	70.0 (6.5)	79.3 (8.6)	
	36.5	47.0	42.9	42.2	
pe					
CNV only		191		156	
GA only		62		10	
Mixed		51		14	
					Me Beta
ug/ml (95% CI)[a]	5.5 (4.9-6.2)	6.6 (6.0-7.2)	6.0 (5.6-6.3)	7.2 (6.6-7.8)	0.19, (x 10 0.3(
ohort association, Beta, SE, *P*[b]	0.18, 0.07, 0.016 (0.17, 0.07, 0.018)		0.19, 0.05, 1.7 x 10^{-4} (0.24, 0.06, 8.4 x 10^{-5})		
ml (95% CI)[a]	349.0 (338.9-359.4)	348.6 (340.2-357.2)	304.7 (297.3-312.2)	308.7 (298.0- 319.8)	0.01, 0.704 0.
ohort association, Beta, SE, *P*[b]	-0.001, 0.2, 0.959 (0.006, 0.02, 0.752)		0.01, 0.02, 0.535 (0.02, 0.02, 0.433)		

[a]FHR-4 and FH levels are expressed as geometric mean values (back-log transformed); [b]Wald tests using linear regression models; adjusted P-values for sex, age, batch effects and first two genetic principal components are displayed in parentheses

Table 2. Single-variant association analyses with FHR-4 and FH levels for the 8 AMD independently associated variants at the *CFH* locus from the IAMDGC study[5].

	Cambridge				EUGENDA				Me
	MAF		Association with FHR-4 levels[a]	Association with FH levels[a]	MAF		Association with FHR-4 levels[a]	Association with FH levels[a]	Associat with FHR-4 levels
dbSNP ID hr:Position[c] Major/Minor allele putation R^2)[d]	Controls	Cases	Beta (SE) *P*	Beta (SE) *P*	Controls	Cases	Beta (SE) *P*	Beta (SE) *P*	Beta (SE) *P*
rs10922109 :196704632 C/A (1.00)	0.415	0.208	-0.43 (0.05) 5.8×10^{-16}	0.04 (0.01) 0.003	0.437	0.219	-0.42 (0.03) 3.3×10^{-35}	0.02 (0.02) 0.318	-0.42 (0.03) 2.2×10^{-5}
rs570618 :196657064 G/T (1.00)	0.367	0.599	0.20 (0.05) 3.8×10^{-5}	-0.004 (0.01) 0.783	0.354	0.572	0.24 (0.03) 3.0×10^{-12}	0.01 (0.01) 0.669	0.23 (0.03) 1.6×10^{-1}
s121913059 :196716375 C/T Genotyped)	*Only 1 case heterozygote carrier*				*No T allele carriers*				*Not*
s148553336 :196613173 T/C Genotyped)	0.020	0.002	0.28 (0.27) 0.287	-0.17 (0.07) 0.019	0.004	*No C allele carriers*	*Not analysed*	*Not analysed*	*Not*
s187328863 :196380158 C/T (0.83)	0.010	0.047	0.31 (0.15) 0.038	-0.07 (0.04) 0.107	0.038	0.040	0.35 (0.10) 2.9×10^{-4}	-0.07 (0.04) 0.089	0.34 (0.08) 2.8×10^{-5}
rs61818925 :196815450 G/T (0.87)	0.399	0.276	-0.29 (0.06) 1.8×10^{-7}	-0.01 (0.02) 0.642	0.393	0.315	-0.29 (0.04) 3.3×10^{-15}	-0.06 (0.02) 4.3×10^{-4}	-0.29 (0.03) 2.8×10^{-2}
rs35292876 :196706642 C/T Genotyped)	0.005	0.016	-0.05 (0.23) 0.815	-0.11 (0.06) 0.090	0.008	0.025	0.32 (0.14) 0.019	0.04 (0.06) 0.517	0.22 (0.12) 0.057
s191281603 :196958651 C/G (0.42)	0.009	0.007	0.11 (0.46) 0.812	-0.09 (0.13) 0.490	0.010	0.008	0.23 (0.25) 0.357	0.24 (0.11) 0.025	0.20 (0.22) 0.357

MAF, Minor Allele Frequency; Chr, chromosome; SE, Standard Error; IAMDGC, International Age-related Macular Degeneration Genomics Consortium study[5].

[a]Wald tests using linear regression models adjusted for AMD status, sex, age, batch effects and the first two ancestry principal components (as estimated within the IAMDGC study[5]); [b]direction of association with AMD for the minor allele, as estimated in the IAMDGC study[5]; [c]Chromosomal position is given according to the NCBI RefSeq hg19 human genome reference assembly. Bonferroni correction for multiple testing of 8 variants = 0.00625 (0.05/8). [d]Imputation quality metric R^2 as estimated in the IAMDGC study[5].

SUPPLEMENTARY INFORMATION

Factor H-Related Protein 4 helps drive complement activation in age-related macular degeneration

Valentina Cipriani[1,2,3,4,16,*], Laura Lorés-Motta[5,16], Fan He[6], Dina Fathalla[7], Viranga Tilakaratna[6], Selina McHarg[6], Nadhim Bayatti[6], İlhan E. Acar[5], Carel B. Hoyng[5], Sascha Fauser[8,9], Anthony T. Moore[1,2,10], John RW Yates[1,2,11], International Age-related Macular Degeneration Genomics Consortium (IAMDGC), Eiko K de Jong[5], B. Paul Morgan[7,17], Anneke I. den Hollander[5,12,17], Paul N. Bishop[6,13,17], Simon J. Clark[6,14,15,17,*]

[1]UCL Institute of Ophthalmology, University College London, London, EC1V 9EL, UK.

[2]Moorfields Eye Hospital NHS Foundation Trust, London, EC1V 2PD, UK.

[3]UCL Genetics Institute, University College London, London, WC1E 6BT, UK.

[4]William Harvey Research Institute, Clinical Pharmacology, Queen Mary University of London, London, EC1M 6BQ, UK.

[5]Department of Ophthalmology, Donders Institute for Brain, Cognition and Behaviour, Radboud university medical centre, Nijmegen, 6525 HR, the Netherlands.

[6]Division of Evolution and Genomic Sciences, School of Biological Sciences, Faculty of Biology Medicine and Health, University of Manchester, Oxford Road, Manchester, M13 9PT, UK.

[7]Systems Immunity URI, Division of Infection and Immunity, and UK DRI Cardiff, School of Medicine, Cardiff University, Cardiff, CF14 4XN, UK.

[8]Department of Ophthalmology, University Hospital of Cologne, Cologne, 50924, Germany.

[9]Roche Pharma Research and Early Development, F. Hoffmann-La Roche Ltd, Basel, CH-4070, Switzerland.

[10]Ophthalmology Department, University of California San Francisco, San Francisco, California.

[11]Department of Medical Genetics, University of Cambridge, Cambridge, CB2 0QQ, UK.

[12]Department of Human Genetics, Donders Institute for Brain, Cognition and Behaviour, Radboud university medical centre, Nijmegen, 6525 HR, the Netherlands.

[13]Manchester Royal Eye Hospital, Manchester University NHS Foundation Trust, Manchester Academic Health Science Centre, M13 9WL, UK.

[14]The Lydia Becker Institute of Immunology and Inflammation, Faculty of Biology, Medicine and Health, University of Manchester, Manchester, UK

[15]Current address: Research Institute of Ophthalmology, Department of Ophthalmology, Eberhard Karls University of Tübingen, 72076 Tübingen, Germany

[16]These authors contributed equally to this work.

[17]These authors jointly supervised this work.

[*]Correspondence should be addressed to: V.C. (v.cipriani@qmul.ac.uk) or S.J.C. (simon.clark@uni-tuebingen.de)

Table of Contents

Supplementary Methods 47

Study samples 47

Supplementary Figure 1. Two-stage, fixed-effects meta-analysis of individual participant data from Cambridge and EUGENDA studies shows significant association of FHR-4 levels and late AMD. 48

Supplementary Figure 2. CFHR4 gene transcription was not detected in eye tissues. 49

Supplementary Figure 3. FHR-4 does not diffuse freely across Bruch's membrane. 50

Supplementary Figure 4. FHL-1 mediated C3b breakdown assay. 51

Supplementary Figure 5. Box plots of FHR-4 and FH levels measured in Cambridge and EUGENDA samples, by AMD status and genotype of 8 independently associated variants at the *CFH* locus from the IAMDGC study.[4] 52

Supplementary Figure 6. GWAS meta-analysis of FHR-4 levels in controls reveals a strong genome-wide significant signal spanning the *CFH* locus. 56

Supplementary Figure 7. Association analyses of the common diplotypes (haplotype pairs, with overall frequency ≥ 1%) formed by the 7 AMD independently associated variants at the *CFH* locus considered in our study and rs6677604 (proxy for the previously reported AMD protective *CFHR1-3* deletion[5]) with AMD, FHR-4 and FH levels. 58

Supplementary Figure 8. FHR-4 and FH levels are dictated by a different genetic architecture. 60

Supplementary Figure 9. Sequence of FHR-4 recombinant protein. 61

Supplementary Figure 10. Specificity of anti-FHR-4 antibody. 62

Supplementary Figure 11. Competition ELISA demonstrating specificity of anti-FHR4 antibody clone 150 for FHR-4 over FH. 64

List of the IAMDGC members 65

Supplementary References 70

Supplementary Methods

Study samples

Cambridge AMD study patients were excluded if they had greater than 6 diopters of myopic refractive error or evidence of other inflammatory or retinovascular disease (such as retinal vessel occlusion, diabetic retinopathy, or chorioretinitis) that could contribute to the development of or confound the diagnosis of maculopathy. All participants described their race/ethnicity as white on a recruitment questionnaire and were confirmed to be of European descent in the genetic analyses. Participants were examined by an ophthalmologist and underwent color stereoscopic fundus photography of the macular region. Images were graded at the Reading Centre, Moorfields Eye Hospital, London, using the International Classification of Age-related Maculopathy and Macular Degeneration.[1]

For the European Genetic Database (EUGENDA) cohort, all the individuals were graded by classification of retinal images according to the standard protocol of the Cologne Image Reading Center by certified graders.[2] Only patients graded as late AMD were included in the study. Serum was obtained by a standard coagulation/centrifugation protocol, and within 1 hour after collection serum samples were stored at –80°C.

A

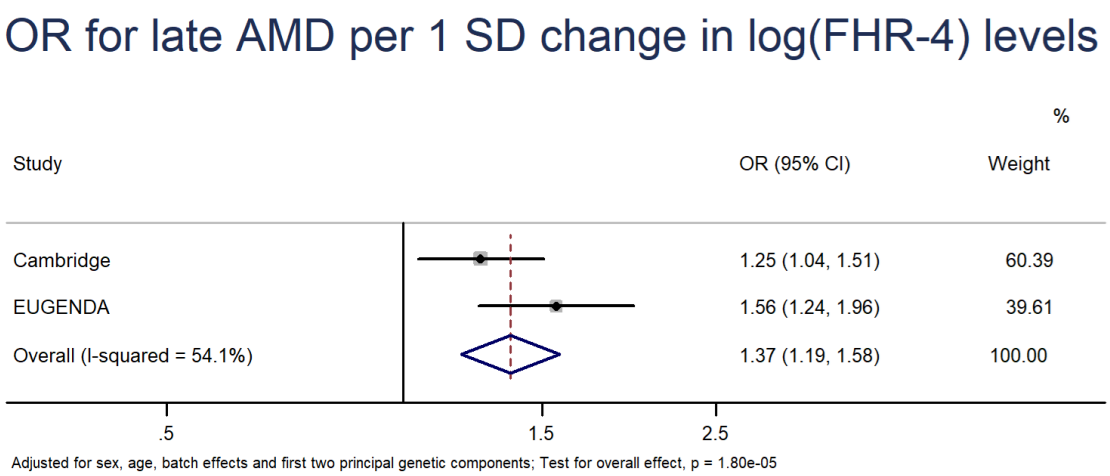

B

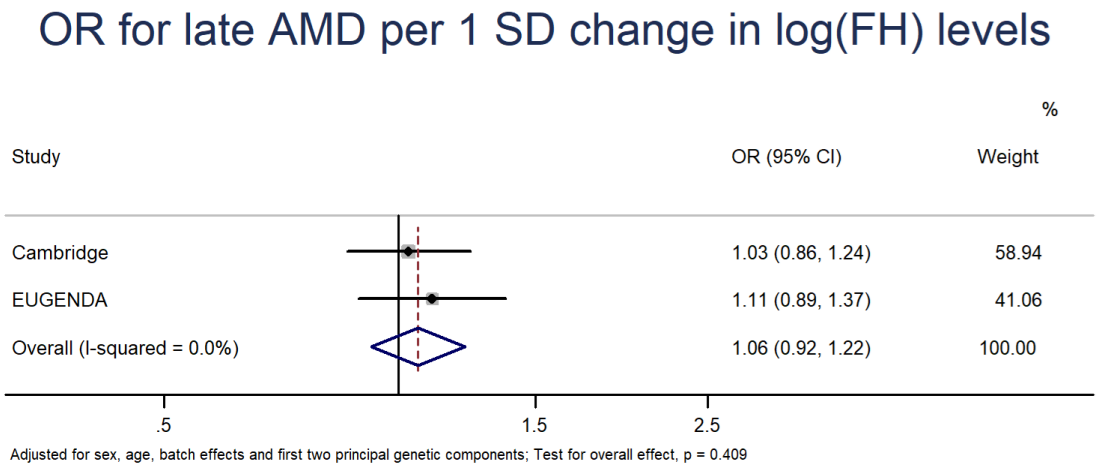

Supplementary Figure 1. Two-stage, fixed-effects meta-analysis of individual participant data from Cambridge and EUGENDA studies shows significant association of FHR-4 levels and late AMD.

Panels A and B show forest plots of odds ratios (ORs) (with 95% Confidence Intervals, CIs) of late AMD per standard deviation (SD) change in natural logarithmically transformed FHR-4 (A) and FH (B) levels using logistic regression models adjusted for sex, age, batch effects and the first two genetic principal components. The overall OR estimate is obtained from a two-stage, fixed-effects meta-analysis of the two study-specific estimates. I^2 statistic is used to assess heterogeneity across studies.

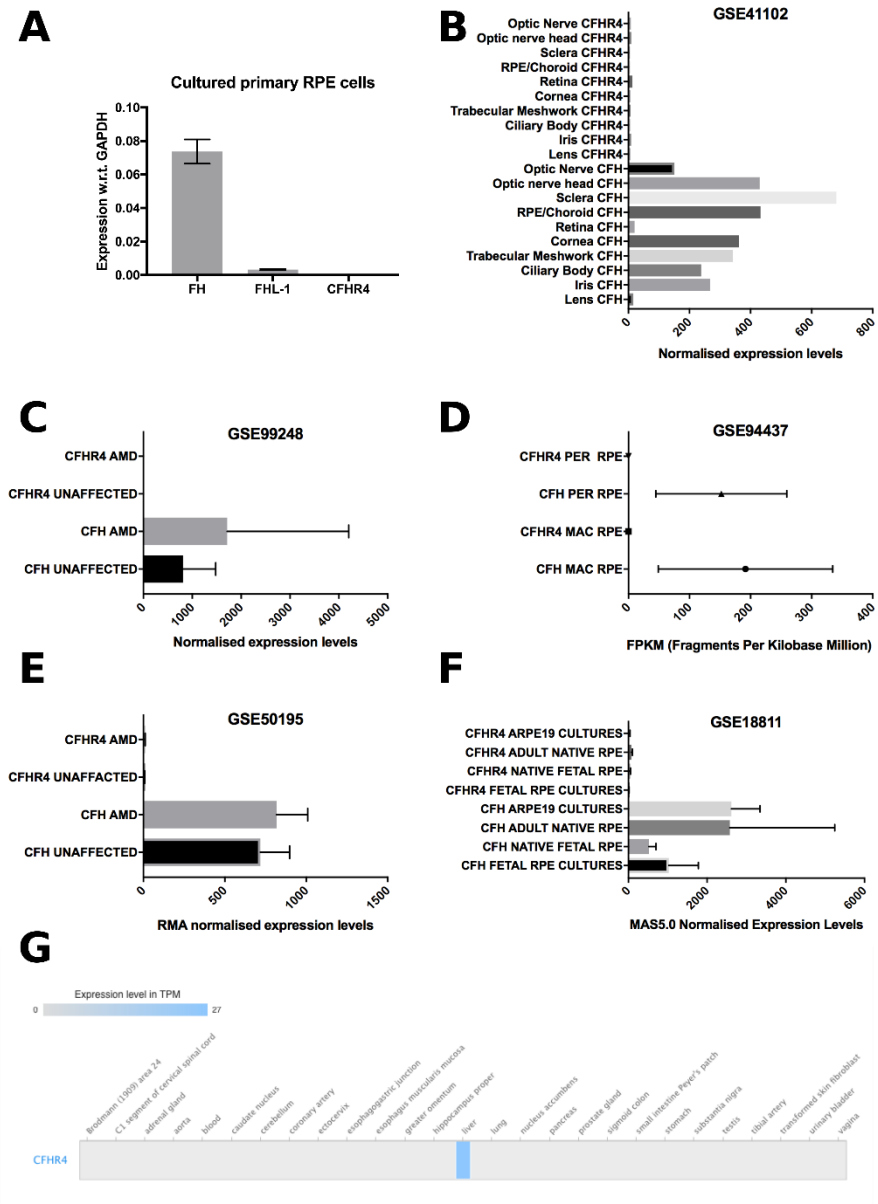

Supplementary Figure 2. CFHR4 gene transcription was not detected in eye tissues. rtPCR analysis on cultured primary human RPE cells from 42 individual donors detects expression of FH and FHL-1, but not FHR-4 (panel A). Panels B-F show data reanalyzed from the NCBI Gene Expression Omnibus public data repository: where B is from an Affymetrix Human Exon 1.0 ST microarray[9]; C, RNAseq (Illumina)[10]; D, RNAseq (Illumina) HiSeq 2000[11]; E, Affymetrix Human Exon 1.0 ST microarray[12]; and F, Affymetrix U133plus2 human genome array[13]. Panel G: RNAseq of 53 human tissue samples from the Genotype-Tissue Expression (GTEx) project[14] detects CFHR4 expression only in the liver. Error bars in panels A-F represent standard deviation. Source data are provided as a Source Data file.

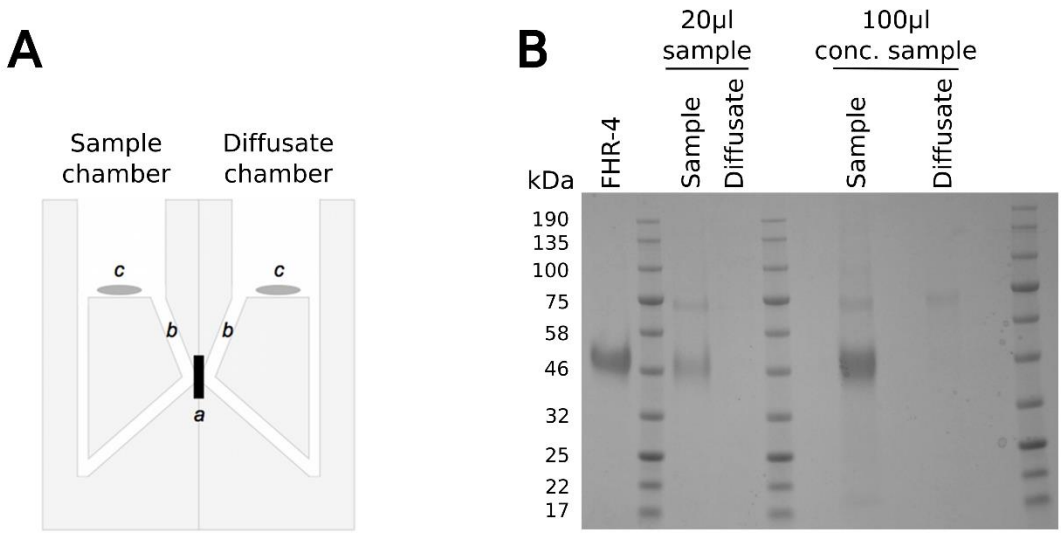

Supplementary Figure 3. FHR-4 does not diffuse freely across Bruch's membrane.
Enriched Bruch's membrane from donor eyes were placed inside a modified Ussing chamber, where: a, is the enriched BrM; b, are the sampling access points; and c, are magnetic stirrer bars to maintain flow around each chamber (panel A). Panel B: samples from either the sample chamber or diffusate chamber were run on a 4-12% NuPage gel Bis-Tris gel and compared to a pure protein control (FHR-4); the protein in the gel was stained with Instant Blue. The gel shows 20µl samples taken and run directly from each chamber, as well as 100µl samples that have been concentrated prior to running on the gel. Gel is representative of three independent experiments.

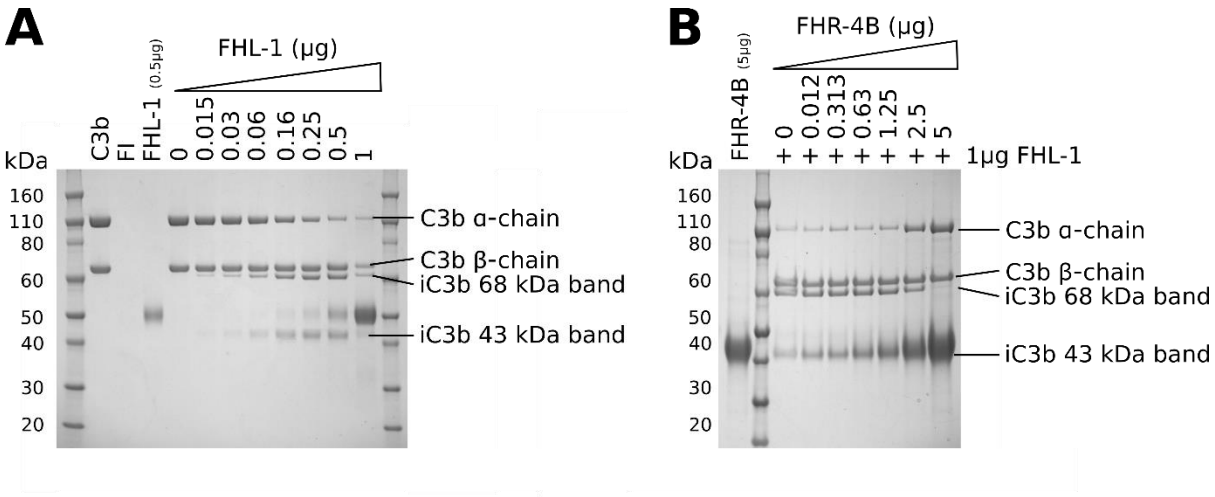

Supplementary Figure 4. FHL-1 mediated C3b breakdown assay.

Panel A: protein stained SDS-PAGE gel demonstrating FI cleavage of C3b in the fluid phase in the presence of a co-factor (FHL-1) is shown, with pure C3b (2µg), FI (0.04µg), and FHL-1 (0.5µg) controls included. FI cannot cleave the α-chain of C3b without a co-factor (lane '0'), but with increasing concentration of FHL-1 the breakdown of the C3b α-chain into iC3b (seen as two bands at 68kDa and 43kDa) was observed. Gel is representative of three independent experiments. Panel B: a repeat of the C3b breakdown assay as shown previously (panel A) but the amount of FHL-1 remains a constant 1µg and increasing amounts of FHR-4B purified protein is supplemented into the reaction. The 43kDa iC3b band is masked by the presence of FHR-4B. This competition assay gel is representative of three independent experiments.

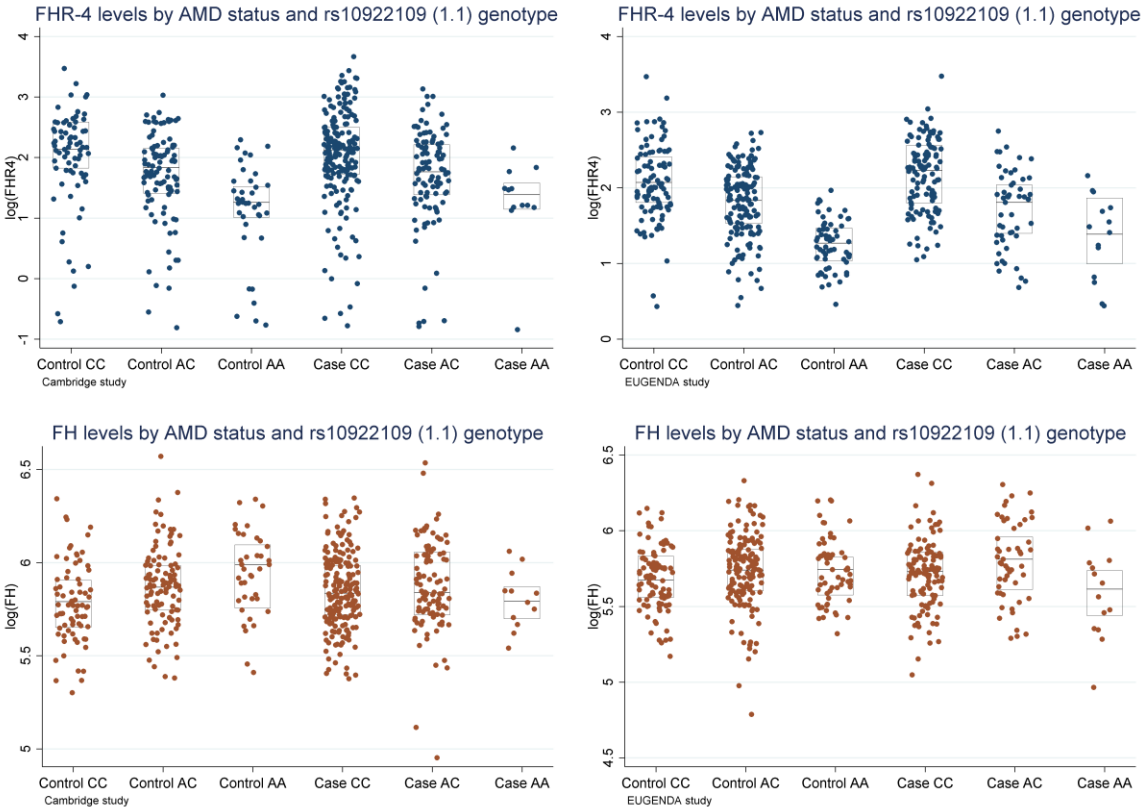

Supplementary Figure 5. Box plots of FHR-4 and FH levels measured in Cambridge and EUGENDA samples, by AMD status and genotype of 8 independently associated variants at the *CFH* locus from the IAMDGC study.[4]

Note: the *CFH* variant rs121913059 (R1210C,[15] IAMDGC association signal number 1.3) was present heterozygously only in a single case from the Cambridge cohort and no corresponding box plot of FHR-4/FH levels is shown.

Source data are provided as a Source Data file.

(continued on the next page)

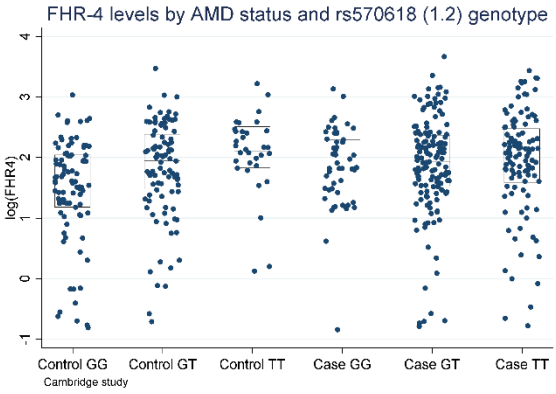

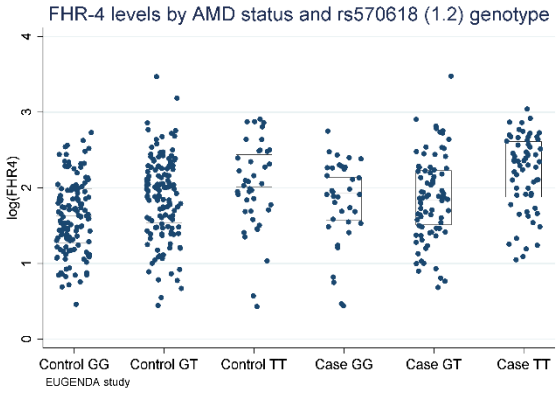

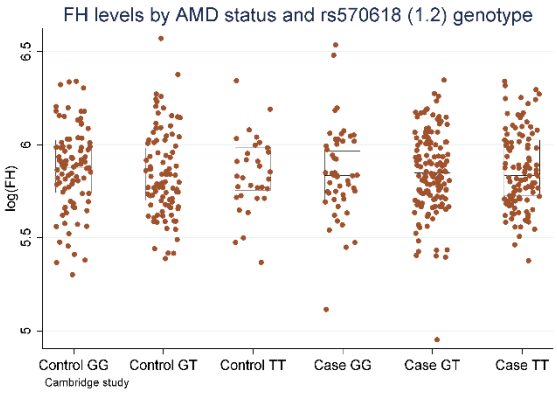

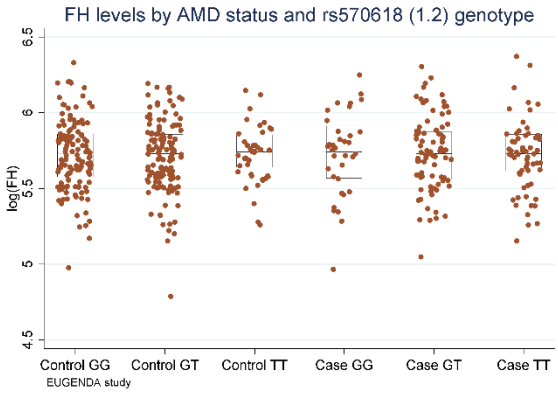

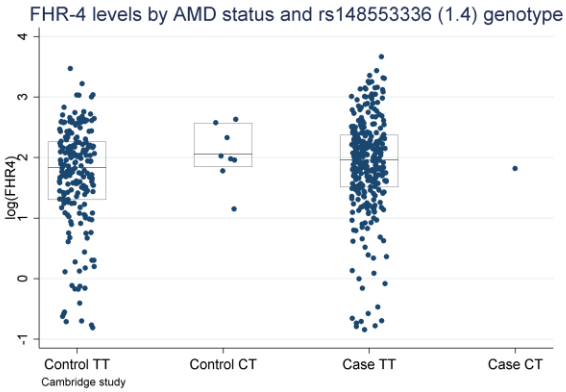

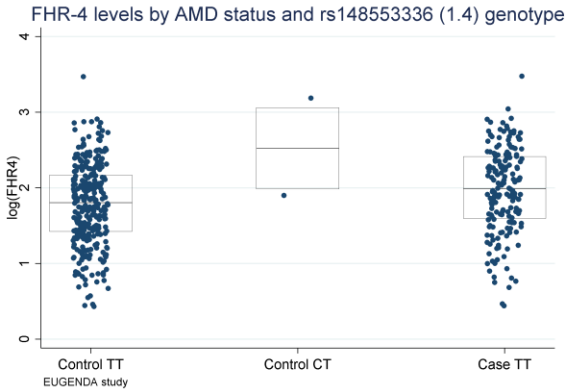

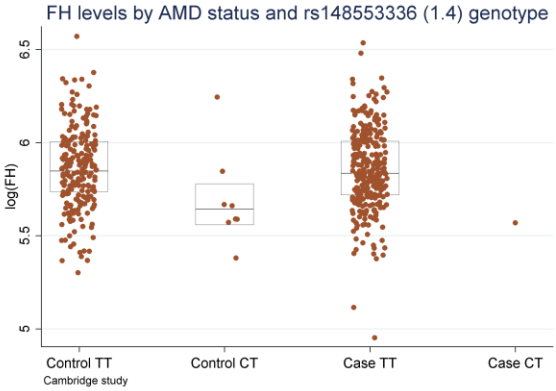

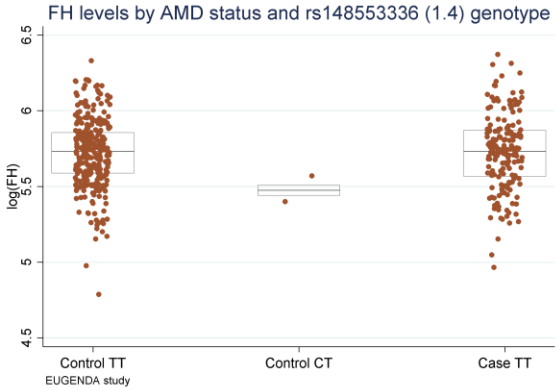

(continued on the next page)

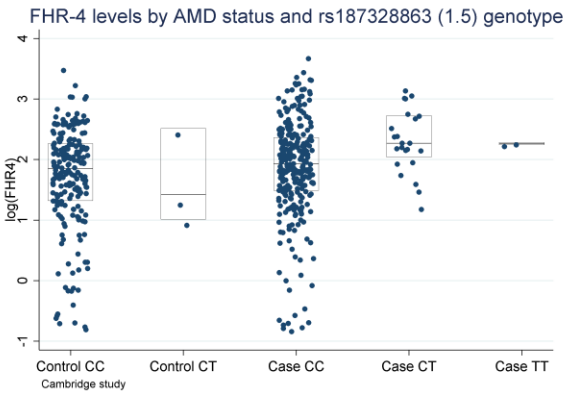

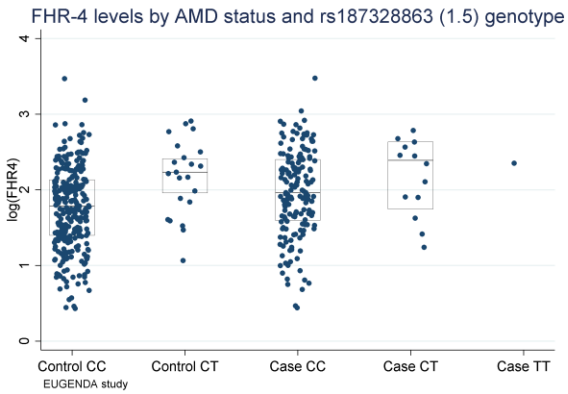

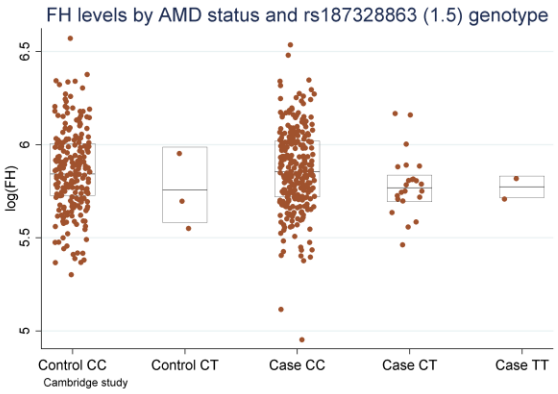

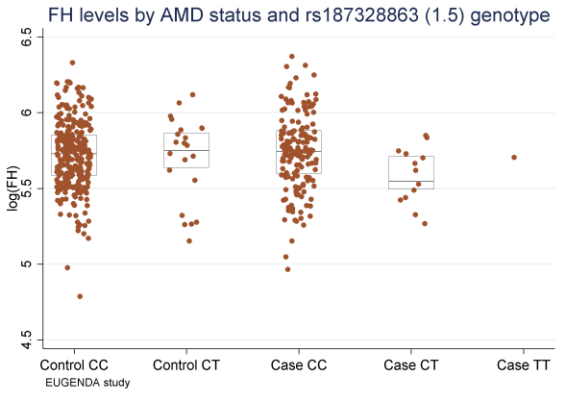

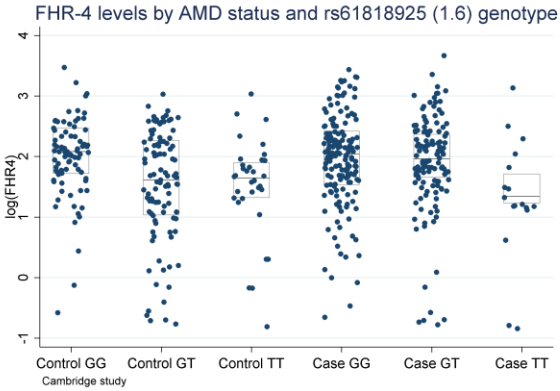

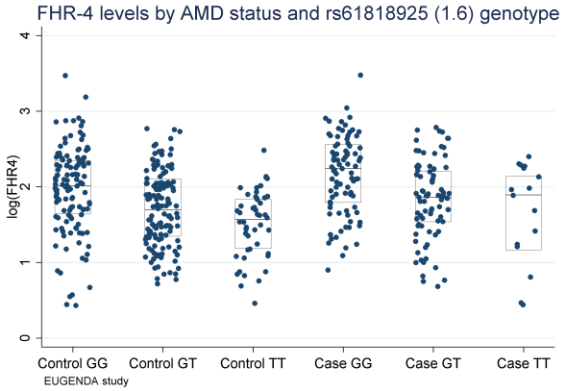

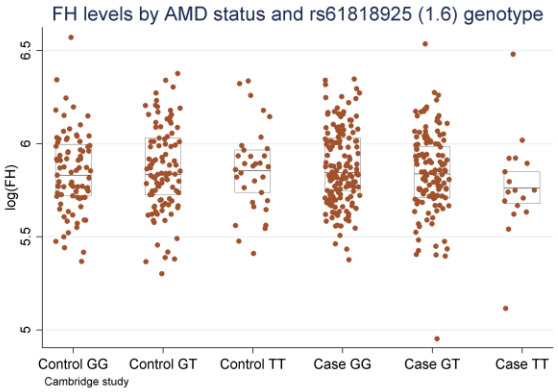

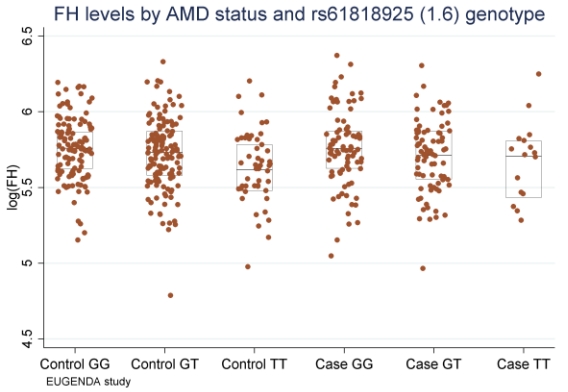

(continued on the next page)

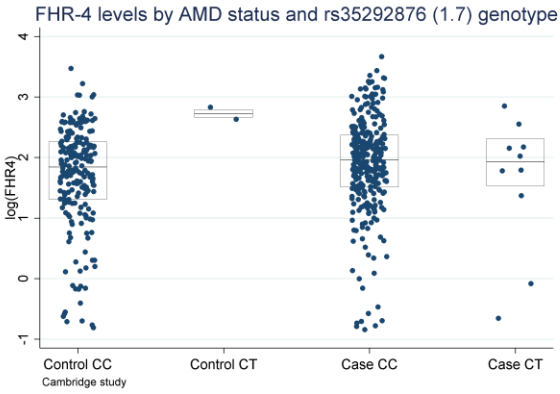
FHR-4 levels by AMD status and rs35292876 (1.7) genotype
log(FHR4)
-1
0
1
2
3
4
Control CC
Control CT
Case CC
Case CT
Cambridge study

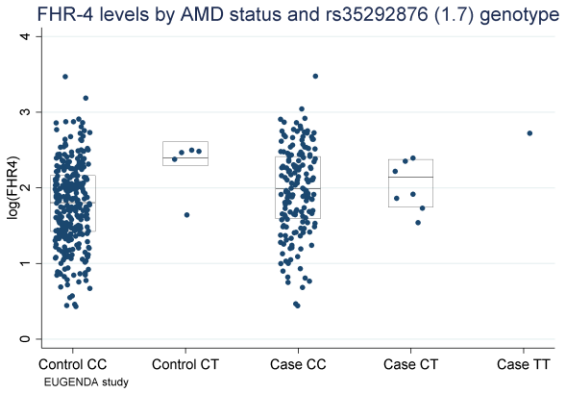
FHR-4 levels by AMD status and rs35292876 (1.7) genotype
log(FHR4)
0
1
2
3
4
Control CC
Control CT
Case CC
Case CT
Case TT
EUGENDA study

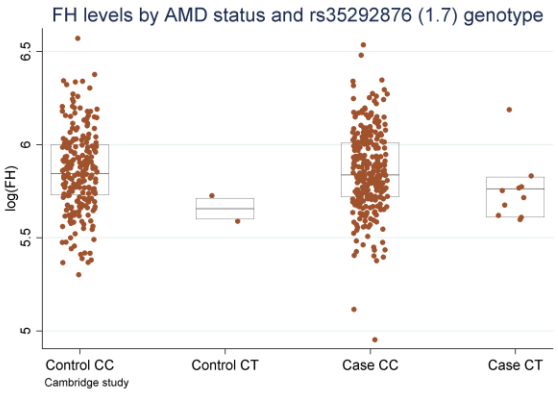
FH levels by AMD status and rs35292876 (1.7) genotype
log(FH)
5
5.5
6
6.5
Control CC
Control CT
Case CC
Case CT
Cambridge study

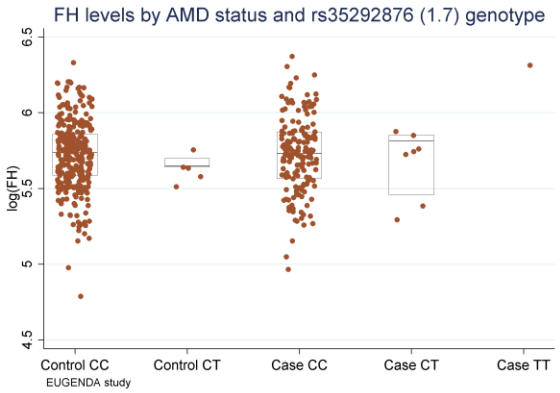
FH levels by AMD status and rs35292876 (1.7) genotype
log(FH)
4.5
5
5.5
6
6.5
Control CC
Control CT
Case CC
Case CT
Case TT
EUGENDA study

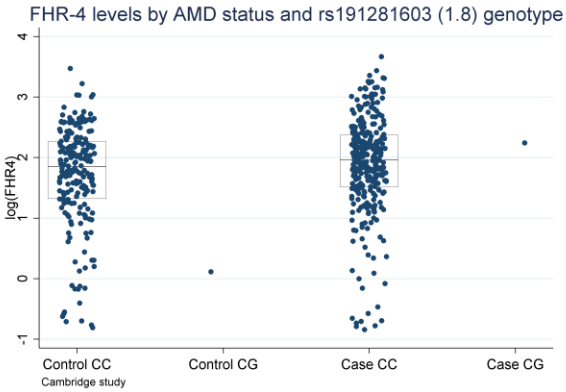
FHR-4 levels by AMD status and rs191281603 (1.8) genotype
log(FHR4)
-1
0
1
2
3
4
Control CC
Control CG
Case CC
Case CG
Cambridge study

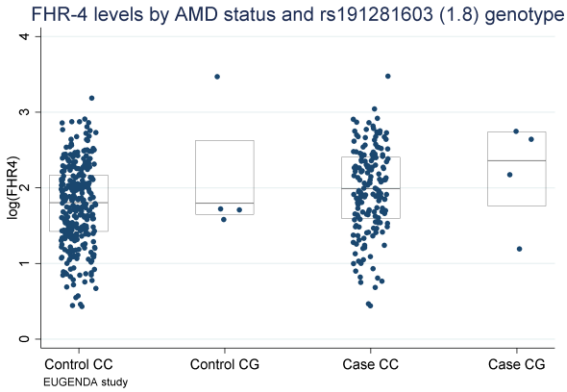
FHR-4 levels by AMD status and rs191281603 (1.8) genotype
log(FHR4)
0
1
2
3
4
Control CC
Control CG
Case CC
Case CG
EUGENDA study

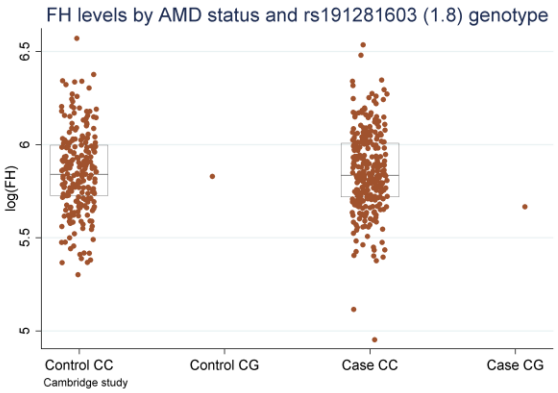
FH levels by AMD status and rs191281603 (1.8) genotype
log(FH)
5
5.5
6
6.5
Control CC
Control CG
Case CC
Case CG
Cambridge study

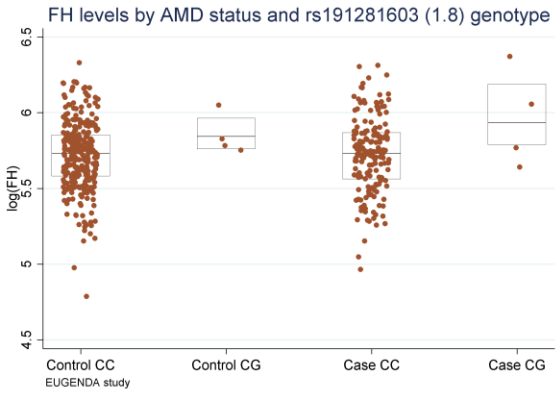
FH levels by AMD status and rs191281603 (1.8) genotype
log(FH)
4.5
5
5.5
6
6.5
Control CC
Control CG
Case CC
Case CG
EUGENDA study

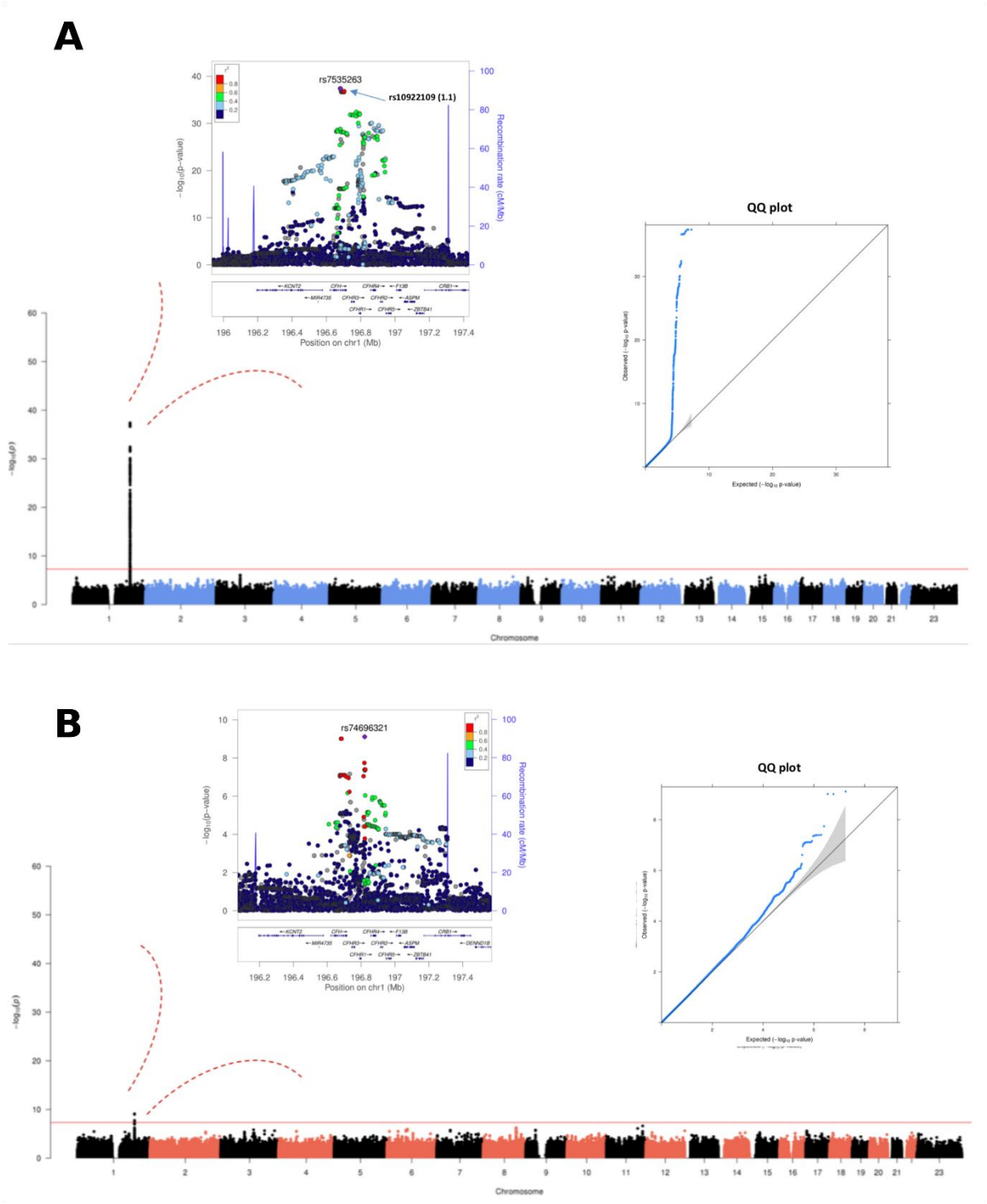

Supplementary Figure 6. GWAS meta-analysis of FHR-4 levels in controls reveals a strong genome-wide significant signal spanning the *CFH* locus.

Each panel shows a Manhattan plot, a regional plot (upper left-hand side) and a quantile-quantile (QQ) plot (upper right-hand side) for the results of the GWAS meta-analysis of FHR-4 levels (Panel A) and FH levels (Panel B). Manhattan plots illustrate P-values for each single variant tested for association with log(levels). Observed -$\log_{10}$(P-values) are plotted against the

genomic position of each variant on chromosomes 1–22 plus the X chromosome. The horizontal red line indicates the threshold considered for genome-wide significance (P-value ≤ 5×10^{-8}). Regional plots show the only genome-wide association signal observed, i.e., at the CFH locus (on chromosome 1q31.3). The most associated variant is denoted by a purple circle and is labelled by its rsID. The other surrounding variants are shown by circles coloured to reflect the extent of LD with the most associated variant (based on 1000 Genomes data, November 2014). A diagram of the genes within the relevant regions is depicted below each plot. Physical positions are based on NCBI RefSeq hg19 human genome reference assembly. QQ plots compare the distribution of the observed test statistics with its expected distribution under the null hypothesis of no association. A marked departure from the null hypothesis (red line) is seen in the meta-analysis of FHR-4 levels (corresponding to the CFH locus). Genomic inflation values (λ) were equal to 1.005 and 0.998 from the GWASs of FHR-4 levels and 0.998 and 0.999 from the GWASs of FH levels, in the Cambridge and EUGENDA studies, respectively.

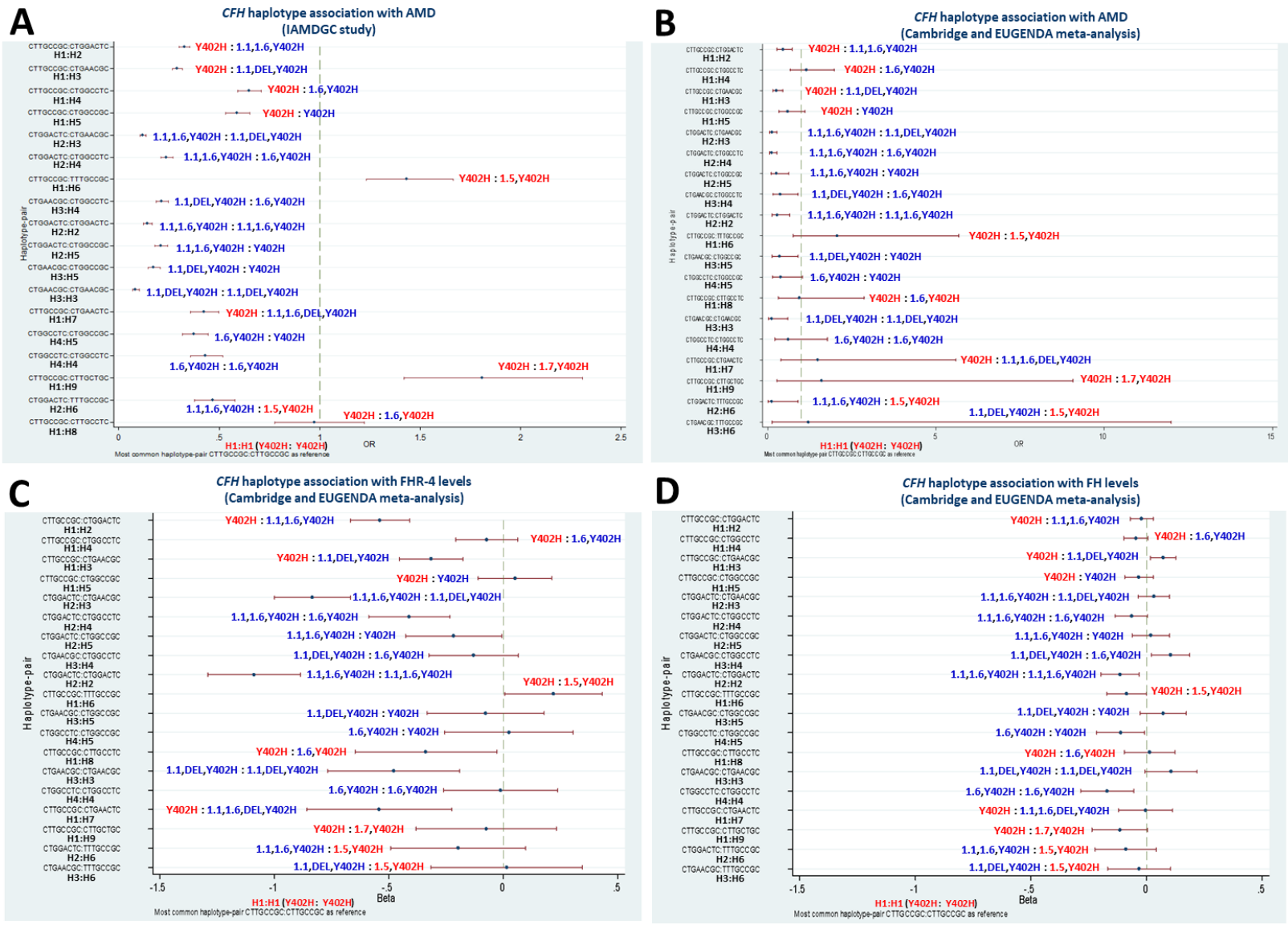

Supplementary Figure 7. Association analyses of the common diplotypes (haplotype pairs, with overall frequency ≥ 1%) formed by the 7

AMD independently associated variants at the *CFH* locus considered in our study and rs6677604 (proxy for the previously reported AMD protective *CFHR1-3* deletion[5]) with AMD, FHR-4 and FH levels.

Panels A and B show the OR (with 95% CI) estimates for the *CFH* diplotype (haplotype-pair) association with AMD in the IAMDGC dataset and the Cambridge and EUGENDA meta-analysis, respectively; panels C and D show the Beta (with 95% CI) estimates for the *CFH* diplotype (haplotype-pair) association with FHR-4 and FH levels, respectively, in the Cambridge and EUGENDA meta-analysis; the haplotype-pair H1:H1 is used as reference. Numerical details together with haplotype-pair frequencies and P-values are given in Supplementary Data 10. The estimates shown in each plot are labelled further according to the presence of the alleles that make each haplotype different from the reference H1, that is indicated with the corresponding IAMDGC association signal numbers (1.1, 1.5-1.7), in red if the allele different from the reference is AMD risk-increasing, in blue if protective; the Y402H label is blue to indicate the presence of the protective allele G of variant 1.2 (rs570618, proxy of Y402H), red for the AMD risk-increasing allele T; finally, the label DEL indicates the presence of the protective allele A of the proxy for the *CFHR1-3* deletion (rs6677604). Source data are provided as a Source Data file.

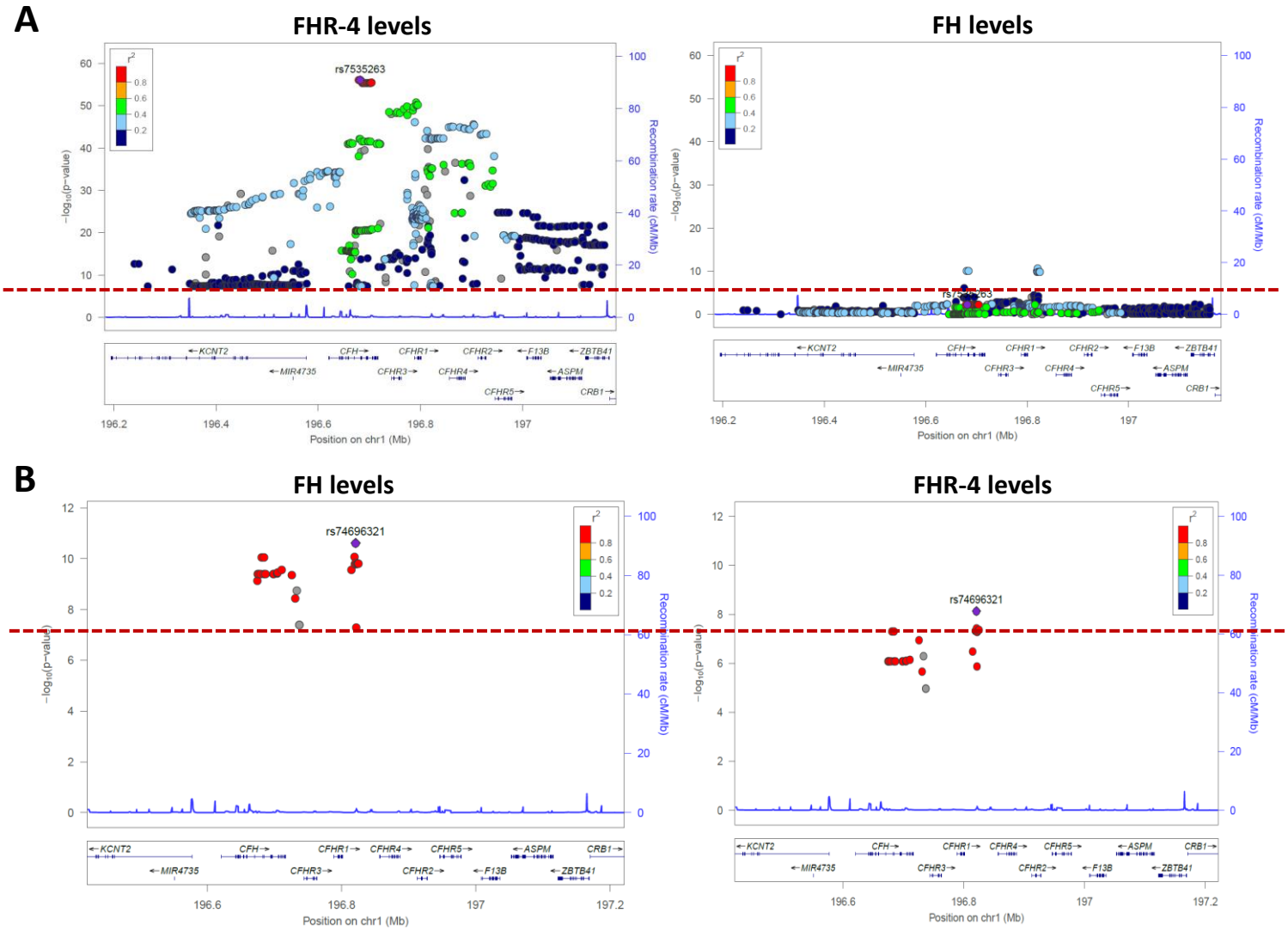

Supplementary Figure 8. FHR-4 and FH levels are dictated by a different genetic architecture.

Regional plots show results from two-cohort (Cambridge and EUGENDA) GWAS meta-analysis of FHR-4 and FH levels only for those variants that showed genome-wide significant (P-value $\leq 5 \times 10^{-8}$) associations with levels of FHR-4 (Panel A) and FH (Panel B). The most associated variant (rs7535263 and rs74696321 for levels of FHR-4 and FH, respectively) is denoted by a purple circle and is labelled by its rsID. The other surrounding variants (811 and 28 for Panel A and B, respectively) are shown by circles coloured to reflect the extent of D with the most associated variant (based on 1000 Genomes data, November 2014). A diagram of the genes within the relevant regions is depicted below each plot. Physical positions are based on NCBI RefSeq hg19 human genome reference assembly.

* ** *** ****

HHHHHHGSSENLYFQGSSGQEVKPCDFPEIQHGGLYYKSLRRLYFPAAAGQSYSYYCDQNF
VTPSGSYWDYIHCTQDGWSPTVPCLRTCSKSDIEIENGFISESSSIYILNKEIQYKCKPGYATAD
GNSSGSITCLQNGWSAQPICIKFCDMPVFENSRAKSNGMRFKLHDTLDYECYDGYEISYGNT
TGSIVCGEDGWSHFPTCYNSSEKCGPPPPISNGDTTSFLLKVYVPQSRVEYQCQSYYELQGSN
YVTCSNGEWSEPPRCIHPCIITEENMNKNNIQLKGKSDIKYYAKTGDTIEFMCKLGYNANTSV
LSFQAVCREGIVEYPRCE

Supplementary Figure 9. Sequence of FHR-4 recombinant protein.

Recombinant FHR-4 gene synthesis was carried out by GenScript using their gene synthesis and protein expression service and is based on the published sequence for the FHR-4B variant of the *CFHR4* gene (UniProt identifier Q92496-3). The original recombinant protein included an N-terminal 6xHis tag (*) followed by, a linker region (**), and a TEV protease cleavage site (***). Removal of the N-terminal His tag results in two non-authentic N-terminal residues (****).

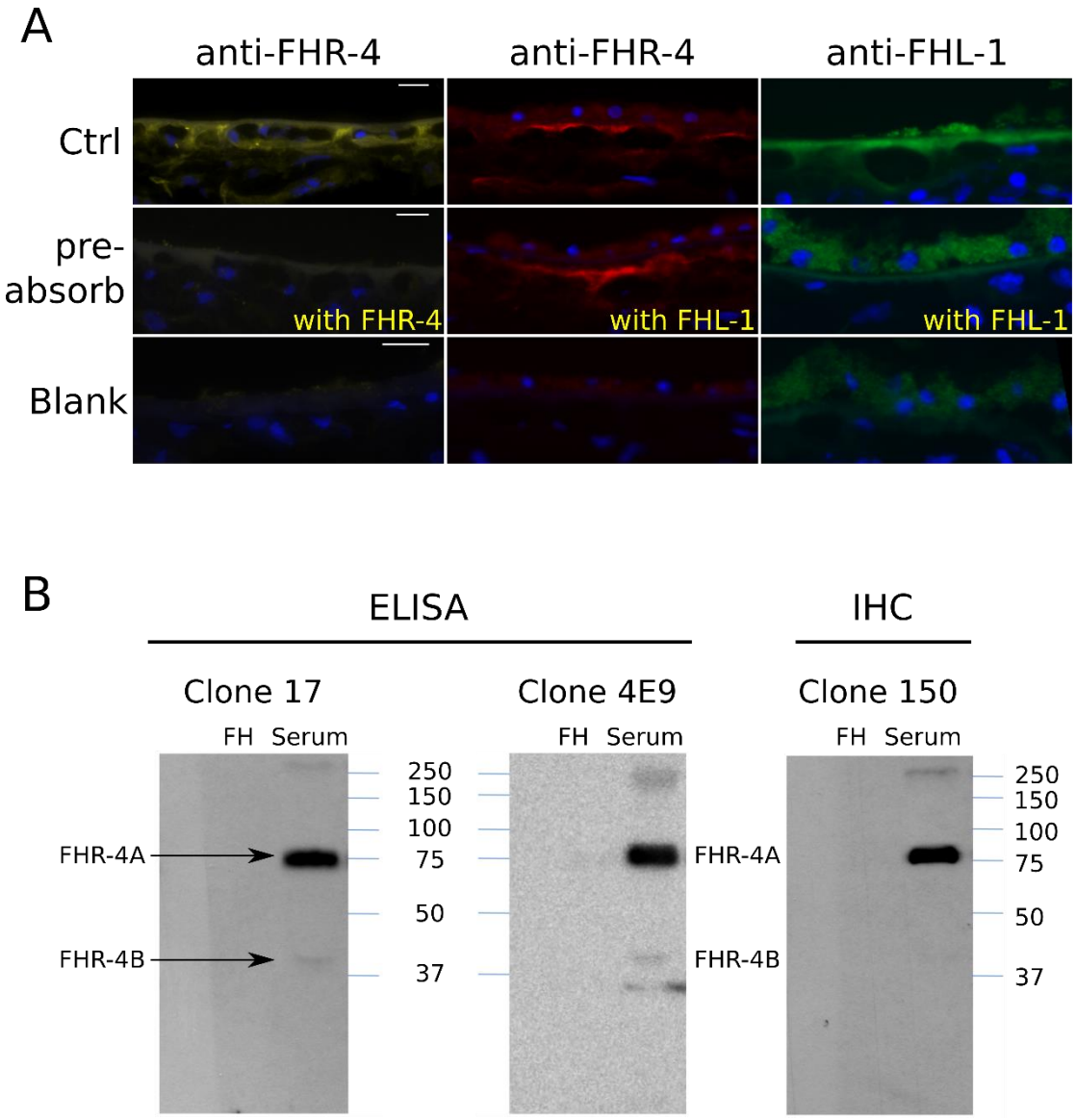

Supplementary Figure 10. Specificity of anti-FHR-4 antibody.

Panel A: the tissue staining specificity of anti-FHR-4 used in our IHC experiments (clone 150) was tested, where the normal 10μg/ml Ab mix used throughout the study was pre-incubated with pure recombinant FHR-4 at a final concentration of 100μg/ml (i.e. 10-fold excess). Staining from the pre-absorption experiments was strikingly similar to the blank controls, where no primary antibody is included. This was repeated with pure FHL-1 protein to demonstrate no cross-reactivity with the antibody existed. The specificity of FHL-1 staining itself with an in-house anti-FHL-1 antibody was also tested, as originally published previously.[16] Panel B: Western blots of non-reduced whole human serum showing three separate clones of anti-FHR-4 antibody with strong reactivity for a band corresponding to FHR-4A, and a faint band corresponding to FHR-4B: the larger FHR-4A has been reported to be the predominant form of FHR-4 in blood.[17] The lanes designated 'FH' had pure factor H protein

loaded to investigate any potential cross-reactivity with the anti-FHR-4 Abs and the full length protein. Source data are provided as a Source Data file.

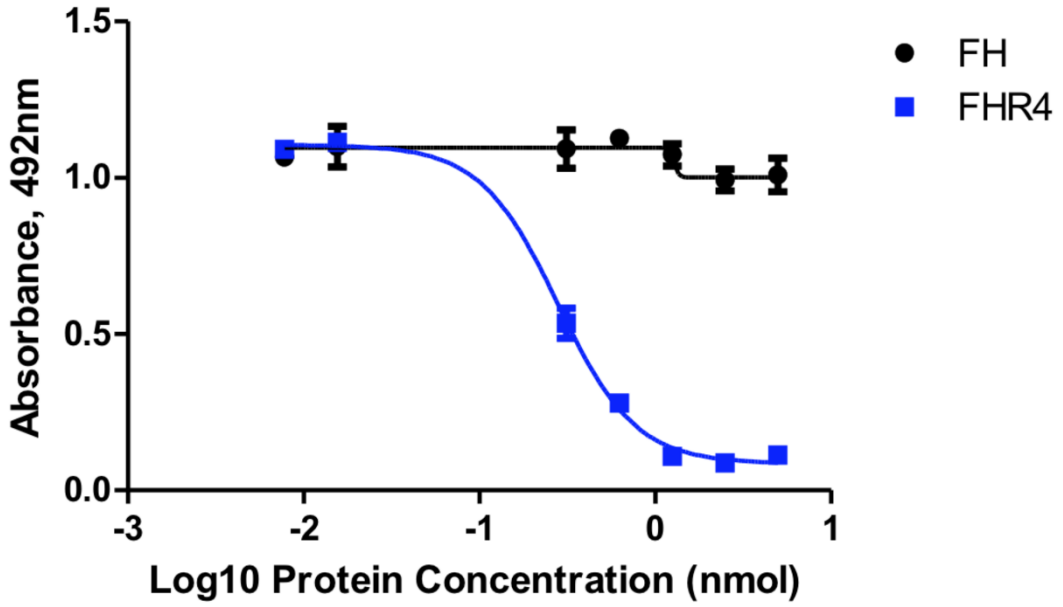

Supplementary Figure 11. Competition ELISA demonstrating specificity of anti-FHR4 antibody clone 150 for FHR-4 over FH.

Immobilised FHR-4 protein was detected by the addition of a saturating dose of the anti-FHR-4 monoclonal antibody used in IHC experiments and ELISA (clone 150). Serial dilutions of either FH (black line) or FHR-4 (blue line) were added in solution together with the anti-FHR-4 antibody. Bound anti-FHR-4 was detected by the addition of anti-mouse IgG HRP-conjugated secondary antibody. Bound secondary antibody detected by addition of OPD substrate and measurement of absorbance at OD492nm. For each data point n=3 and error bars shown are standard error of the mean of the triplicates. Source data are provided as a Source Data file.

List of the IAMDGC members

The list of the IAMDGC members reflects the author list of the previous publication by Fritsche *et al.*, 2016.[4]

Lars G Fritsche[1,100], Wilmar Igl[2,100], Jessica N Cooke Bailey[3,100], Felix Grassmann[4,100], Sebanti Sengupta[1,100], Jennifer L Bragg-Gresham[1,5], Kathryn P Burdon[6], Scott J Hebbring[7], Cindy Wen[8], Mathias Gorski[2], Ivana K Kim[9], David Cho[10], Donald Zack[11-15], Eric Souied[16], Hendrik P N Scholl[11,17], Elisa Bala[18], Kristine E Lee[19], David J Hunter[20,21], Rebecca J Sardell[22], Paul Mitchell[23], Joanna E Merriam[24], Valentina Cipriani[25,26], Joshua D Hoffman[27], Tina Schick[28], Yara T E Lechanteur[29], Robyn H Guymer[30], Matthew P Johnson[31], Yingda Jiang[32], Chloe M Stanton[33], Gabriëlle H S Buitendijk[34,35], Xiaowei Zhan[1,36,37], Alan M Kwong[1], Alexis Boleda[38], Matthew Brooks[38], Linn Gieser[38], Rinki Ratnapriya[38], Kari E Branham[39], Johanna R Foerster[1], John R Heckenlively[39], Mohammad I Othman[39], Brendan J Vote[6], Helena Hai Liang[30], Emmanuelle Souzeau[40], Ian L McAllister[41], Timothy Isaacs[41], Janette Hall[40], Stewart Lake[40], David A Mackey[6,30,41], Ian J Constable[41], Jamie E Craig[40], Terrie E Kitchner[7], Zhenglin Yang[42,43], Zhiguang Su[44], Hongrong Luo[8], Daniel Chen[8], Hong Ouyang[8], Ken Flagg[8], Danni Lin[8], Guanping Mao[8], Henry Ferreyra[8], Klaus Stark[2], Claudia N von Strachwitz[45], Armin Wolf[46], Caroline Brandl[2,4,47], Guenther Rudolph[46], Matthias Olden[2], Margaux A Morrison[48], Denise J Morgan[48], Matthew Schu[49-53], Jeeyun Ahn[54], Giuliana Silvestri[55], Evangelia E Tsironi[56], Kyu Hyung Park[57], Lindsay A Farrer[49-53], Anton Orlin[58], Alexander Brucker[59], Mingyao Li[60], Christine A Curcio[61], Saddek Mohand-Saïd[62-65], José-Alain Sahel[25,62-67], Isabelle Audo[62-64,68], Mustapha Benchaboune[65], Angela J Cree[69], Christina A Rennie[70], Srinivas V Goverdhan[69], Michelle Grunin[71], Shira Hagbi-Levi[71], Peter Campochiaro[11,13], Nicholas Katsanis[72-74], Frank G Holz[17], Frédéric Blond[62-64], Hélène Blanché[75], Jean-François Deleuze[75,76], Robert P Igo Jr[3], Barbara Truitt[3], Neal S Peachey[18,77], Stacy M Meuer[19], Chelsea E Myers[19], Emily L Moore[19], Ronald Klein[19], Michael A Hauser[78-80], Eric A Postel[78], Monique D Courtenay[22], Stephen G Schwartz[81], Jaclyn L Kovach[81], William K Scott[22], Gerald Liew[23], Ava G Tan[23], Bamini Gopinath[23], John C Merriam[24], R Theodore Smith[24,82], Jane C Khan[41,83,84], Humma Shahid[84,85], Anthony T Moore[25,26,86], J Allie McGrath[27], Reneé Laux[3], Milam A Brantley Jr[87], Anita Agarwal[87], Lebriz Ersoy[28], Albert Caramoy[28], Thomas Langmann[28], Nicole T M Saksens[29], Eiko K de Jong[29], Carel B Hoyng[29], Melinda S Cain[30], Andrea J Richardson[30], Tammy M Martin[88], John Blangero[31], Daniel E Weeks[32,89], Bal Dhillon[90], Cornelia M van Duijn[35], Kimberly F Doheny[91], Jane Romm[91], Caroline C W

Klaver[34,35], Caroline Hayward[33], Michael B Gorin[92,93], Michael L Klein[88], Paul N Baird[30], Anneke I den Hollander[29,94], Sascha Fauser[28], John R W Yates[25,26,84], Rando Allikmets[24,95], Jie Jin Wang[23], Debra A Schaumberg[20,96,97], Barbara E K Klein[19], Stephanie A Hagstrom[77], Itay Chowers[71], Andrew J Lotery[69], Thierry Léveillard[62-64], Kang Zhang[8,44], Murray H Brilliant[7], Alex W Hewitt[6,30,41], Anand Swaroop[38], Emily Y Chew[98], Margaret A Pericak-Vance[22,101], Margaret DeAngelis[48,101], Dwight Stambolian[10,101], Jonathan L Haines[3,99,101], Sudha K Iyengar[3,101], Bernhard H F Weber[4,101], Gonçalo R Abecasis[1,101] & Iris M Heid[2,101]

[1]Center for Statistical Genetics, Department of Biostatistics, University of Michigan, Ann Arbor, Michigan, USA. [2]Department of Genetic Epidemiology, University of Regensburg, Regensburg, Germany. [3]Department of Epidemiology and Biostatistics, Case Western Reserve University School of Medicine, Cleveland, Ohio, USA. [4]Institute of Human Genetics, University of Regensburg, Regensburg, Germany. [5]Kidney Epidemiology and Cost Center, Department of Internal Medicine–Nephrology, University of Michigan, Ann Arbor, Michigan, USA. [6]School of Medicine, Menzies Research Institute Tasmania, University of Tasmania, Hobart, Tasmania, Australia. [7]Center for Human Genetics, Marshfield Clinic Research Foundation, Marshfield, Wisconsin, USA. [8]Department of Ophthalmology, University of California, San Diego and Veterans Affairs San Diego Health System, La Jolla, California, USA. [9]Retina Service, Massachusetts Eye and Ear, Department of Ophthalmology, Harvard Medical School, Boston, Massachusetts, USA. [10]Department of Ophthalmology, Perelman School of Medicine, University of Pennsylvania, Philadelphia, Pennsylvania, USA. [11]Department of Ophthalmology, Wilmer Eye Institute, Johns Hopkins University School of Medicine, Baltimore, Maryland, USA. [12]Department of Molecular Biology and Genetics, Johns Hopkins University School of Medicine, Baltimore, Maryland, USA. [13]Department of Neuroscience, Johns Hopkins University School of Medicine, Baltimore, Maryland, USA. [14]Institute of Genetic Medicine, Johns Hopkins University School of Medicine, Baltimore, Maryland, USA. [15]Institue de la Vision, Université Pierre et Marie Curie, Paris, France. [16]Hôpital Intercommunal de Créteil, Hôpital Henri Mondor, Université Paris Est Créteil, Créteil, France. [17]Department of Ophthalmology, University of Bonn, Bonn, Germany. [18]Louis Stokes Cleveland Veterans Affairs Medical Center, Cleveland, Ohio, USA. [19]Department of Ophthalmology and Visual Sciences, University of Wisconsin, Madison, Wisconsin, USA. [20]Department of Epidemiology, Harvard School of Public Health, Boston, Massachusetts, USA. [21]Department of Nutrition, Harvard School of Public Health, Boston, Massachusetts, USA. [22]John P. Hussman Institute for Human Genomics, Miller School of Medicine,

University of Miami, Miami, Florida, USA. [23]Centre for Vision Research, Department of Ophthalmology and Westmead Millennium Institute for Medical Research, University of Sydney, Sydney, New South Wales, Australia. [24]Department of Ophthalmology, Columbia University, New York, New York, USA. [25]University College London Institute of Ophthalmology, University College London, London, UK. [26]Moorfields Eye Hospital, London, UK. [27]Center for Human Genetics Research, Vanderbilt University Medical Center, Nashville, Tennessee, USA. [28]Department of Ophthalmology, University Hospital of Cologne, Cologne, Germany. [29]Department of Ophthalmology, Radboud University Medical Centre, Nijmegen, the Netherlands. [30]Centre for Eye Research Australia, University of Melbourne, Royal Victorian Eye and Ear Hospital, East Melbourne, Victoria, Australia. [31]South Texas Diabetes and Obesity Institute, School of Medicine, University of Texas Rio Grande Valley, Brownsville, Texas, USA. [32]Department of Biostatistics, Graduate School of Public Health, University of Pittsburgh, Pittsburgh, Pennsylvania, USA. [33]Medical Research Council (MRC) Human Genetics Unit, Institute of Genetics and Molecular Medicine, University of Edinburgh, Edinburgh, UK. [34]Department of Ophthalmology, Erasmus Medical Center, Rotterdam, the Netherlands. [35]Department of Epidemiology, Erasmus Medical Center, Rotterdam, the Netherlands. [36]Quantitative Biomedical Research Center, Department of Clinical Science, University of Texas Southwestern Medical Center, Dallas, Texas, USA. [37]Center for the Genetics of Host Defense, University of Texas Southwestern Medical Center, Dallas, Texas, USA. [38]Neurobiology, Neurodegeneration and Repair Laboratory (N-NRL), National Eye Institute, US National Institutes of Health, Bethesda, Maryland, USA. [39]Department of Ophthalmology and Visual Sciences, University of Michigan, Kellogg Eye Center, Ann Arbor, Michigan, USA. [40]Department of Ophthalmology, Flinders Medical Centre, Flinders University, Adelaide, South Australia, Australia. [41]Centre for Ophthalmology and Visual Science, Lions Eye Institute, University of Western Australia, Perth, Western Australia, Australia. [42]Sichuan Provincial Key Laboratory for Human Disease Gene Study, Hospital of the University of Electronic Science and Technology of China and Sichuan Provincial People's Hospital, Chengdu, China. [43]Sichuan Translational Medicine Hospital, Chinese Academy of Sciences, Chengdu, China. [44]Molecular Medicine Research Center, State Key Laboratory of Biotherapy, West China Hospital, Sichuan University, Chengdu, China. [45]EyeCentre Southwest, Stuttgart, Germany. [46]University Eye Clinic, Ludwig Maximilians University, Munich, Germany. [47]Department of Ophthalmology, University Hospital Regensburg, Regensburg, Germany. [48]Department of Ophthalmology and Visual Sciences, University of Utah, Salt Lake City, Utah, USA. [49]Department of Medicine (Biomedical Genetics), Boston

University Schools of Medicine and Public Health, Boston, Massachusetts, USA. [50]Department of Ophthalmology, Boston University Schools of Medicine and Public Health, Boston, Massachusetts, USA. [51]Department of Neurology, Boston University Schools of Medicine and Public Health, Boston, Massachusetts, USA. [52]Department of Epidemiology, Boston University Schools of Medicine and Public Health, Boston, Massachusetts, USA. [53]Department of Biostatistics, Boston University Schools of Medicine and Public Health, Boston, Massachusetts, USA. [54]Department of Ophthalmology, Seoul Metropolitan Government Seoul National University Boramae Medical Center, Seoul, Republic of Korea. [55]Centre for Experimental Medicine, Queen's University, Belfast, UK. [56]Department of Ophthalmology, University of Thessaly, School of Medicine, Larissa, Greece. [57]Department of Ophthalmology, Seoul National University Bundang Hospital, Seongnam, Republic of Korea. [58]Department of Ophthalmology, Weill Cornell Medical College, New York, New York, USA. [59]Scheie Eye Institute, Department of Ophthalmology, University of Pennsylvania Perelman School of Medicine, Philadelphia, Pennsylvania, USA. [60]Department of Biostatistics and Epidemiology, University of Pennsylvania Perelman School of Medicine, Philadelphia, Pennsylvania, USA. [61]Department of Ophthalmology, University of Alabama at Birmingham, Birmingham, Alabama, USA. [62]INSERM, Paris, France. [63]Institut de la Vision, Department of Genetics, Paris, France. [64]Centre National de la Recherche Scientifique (CNRS), Paris, France. [65]Centre Hospitalier National d'Ophtalmologie des Quinze-Vingts, Paris, France. [66]Fondation Ophtalmologique Adolphe de Rothschild, Paris, France. [67]Académie des Sciences–Institut de France, Paris, France. [68]Department of Molecular Genetics, Institute of Ophthalmology, London, UK. [69]Clinical and Experimental Sciences, Faculty of Medicine, University of Southampton, Southampton, UK. [70]University Hospital Southampton, Southampton, UK. [71]Department of Ophthalmology, Hadassah Hebrew University Medical Center, Jerusalem, Israel. [72]Center for Human Disease Modeling, Duke University, Durham, North Carolina, USA. [73]Department of Cell Biology, Duke University, Durham, North Carolina, USA. [74]Department of Pediatrics, Duke University, Durham, North Carolina, USA. [75]Centre d'Etude du Polymorphisme Humain (CEPH) Fondation Jean Dausset, Paris, France. [76]Commissariat à l'Energie Atomique et aux Energies Alternatives (CEA), Institut de Génomique, Centre National de Génotypage, Evry, France. [77]Cole Eye Institute, Cleveland Clinic, Cleveland, Ohio, USA. [78]Department of Ophthalmology, Duke University Medical Center, Durham, North Carolina, USA. [79]Department of Medicine, Duke University Medical Center, Durham, North Carolina, USA. [80]Duke Molecular Physiology Institute, Duke University Medical Center, Durham, North Carolina, USA. [81]Bascom Palmer Eye Institute, University of Miami Miller

School of Medicine, Naples, Florida, USA. [82]Department of Ophthalmology, New York University School of Medicine, New York, New York, USA. [83]Department of Ophthalmology, Royal Perth Hospital, Perth, Western Australia, Australia. [84]Department of Medical Genetics, Cambridge Institute for Medical Research, University of Cambridge, Cambridge, UK. [85]Department of Ophthalmology, Cambridge University Hospitals National Health Service (NHS) Foundation Trust, Cambridge, UK. [86]Department of Ophthalmology, University of California San Francisco Medical School, San Francisco, California, USA. [87]Department of Ophthalmology and Visual Sciences, Vanderbilt University, Nashville, Tennessee, USA. [88]Casey Eye Institute, Oregon Health and Science University, Portland, Oregon, USA. [89]Department of Human Genetics, Graduate School of Public Health, University of Pittsburgh, Pittsburgh, Pennsylvania, USA. [90]School of Clinical Sciences, University of Edinburgh, Edinburgh, UK. [91]Center for Inherited Disease Research (CIDR) Institute of Genetic Medicine, Johns Hopkins University School of Medicine, Baltimore, Maryland, USA. [92]Department of Ophthalmology, David Geffen School of Medicine, Stein Eye Institute, University of California, Los Angeles, Los Angeles, California, USA. [93]Department of Human Genetics, David Geffen School of Medicine, University of California, Los Angeles, Los Angeles, California, USA. [94]Department of Human Genetics, Radboud University Medical Centre, Nijmegen, the Netherlands. [95]Department of Pathology and Cell Biology, Columbia University, New York, New York, USA. [96]Center for Translational Medicine, Moran Eye Center, University of Utah School of Medicine, Salt Lake City, Utah, USA. [97]Division of Preventive Medicine, Brigham and Women's Hospital, Harvard Medical School, Boston, Massachusetts, USA. [98]Division of Epidemiology and Clinical Applications, Clinical Trials Branch, National Eye Institute, US National Institutes of Health, Bethesda, Maryland, USA. [99]Institute for Computational Biology, Case Western Reserve University School of Medicine, Cleveland, Ohio, USA.

[100]These authors contributed equally to this work. [101]These authors jointly supervised this work.

Supplementary References

1. Bird, A.C*., et al.* An international classification and grading system for age-related maculopathy and age-related macular degeneration. *Survey of Ophthalmology* **39**, 367-374 (1995).
2. Mokwa, N.F*., et al.* Grading of Age-Related Macular Degeneration: Comparison between Color Fundus Photography, Fluorescein Angiography, and Spectral Domain Optical Coherence Tomography. *J Ophthalmol* (2013).
3. Abecasis, G.R*., et al.* An integrated map of genetic variation from 1,092 human genomes. *Nature* **491**, 56-65 (2012).
4. Fritsche, L.G*., et al.* A large genome-wide association study of age-related macular degeneration highlights contributions of rare and common variants. *Nat Genet* **48**, 134-143 (2016).
5. Hughes, A.E*., et al.* A common CFH haplotype, with deletion of CFHR1 and CFHR3, is associated with lower risk of age-related macular degeneration. *Nature Genetics* **38**, 1173-1177 (2006).
6. Devlin, B. & Roeder, K. Genomic control for association studies. *Biometrics* **55**, 997-1004 (1999).
7. Willer, C.J., Li, Y. & Abecasis, G.R. METAL: fast and efficient meta-analysis of genomewide association scans. *Bioinformatics* **26**, 2190-2191 (2010).
8. Pruim, R.J*., et al.* LocusZoom: regional visualization of genome-wide association scan results. *Bioinformatics* **26**, 2336-2337 (2010).
9. Wagner, A.H*., et al.* Exon-level expression profiling of ocular tissues. *Exp Eye Res* **111**, 105-111 (2013).
10. Kim, E.J*., et al.* Complete Transcriptome Profiling of Normal and Age-Related Macular Degeneration Eye Tissues Reveals Dysregulation of Anti-Sense Transcription. *Scientific Reports* **8**, 3040 (2018).
11. Li, M.Y*., et al.* Comprehensive analysis of gene expression in human retina and supporting tissues. *Human Molecular Genetics* **23**, 4001-4014 (2014).
12. Whitmore, S.S*., et al.* Altered gene expression in dry age-related macular degeneration suggests early loss of choroidal endothelial cells. *Molecular Vision* **19**, 2274-2297 (2013).
13. Strunnikova, N.V*., et al.* Transcriptome analysis and molecular signature of human retinal pigment epithelium. *Human Molecular Genetics* **19**, 2468-2486 (2010).
14. GTEx Consortium. Human genomics. The Genotype-Tissue Expression (GTEx) pilot analysis: multitissue gene regulation in humans. *Science* **348**, 648-660 (2015).
15. Raychaudhuri, S*., et al.* A rare penetrant mutation in CFH confers high risk of age-related macular degeneration. *Nat Genet* **43**, 1232-1236 (2011).
16. Clark, S.J*., et al.* Identification of Factor H-like Protein 1 as the Predominant Complement Regulator in Bruch's Membrane: Implications for Age-Related Macular Degeneration. *J Immunol* **193**, 4962-4970 (2014).
17. Pouw, R.B*., et al.* Complement Factor H-Related Protein 4A Is the Dominant Circulating Splice Variant of CFHR4. *Frontiers in Immunology* **9**(2018).

33

Figure 1

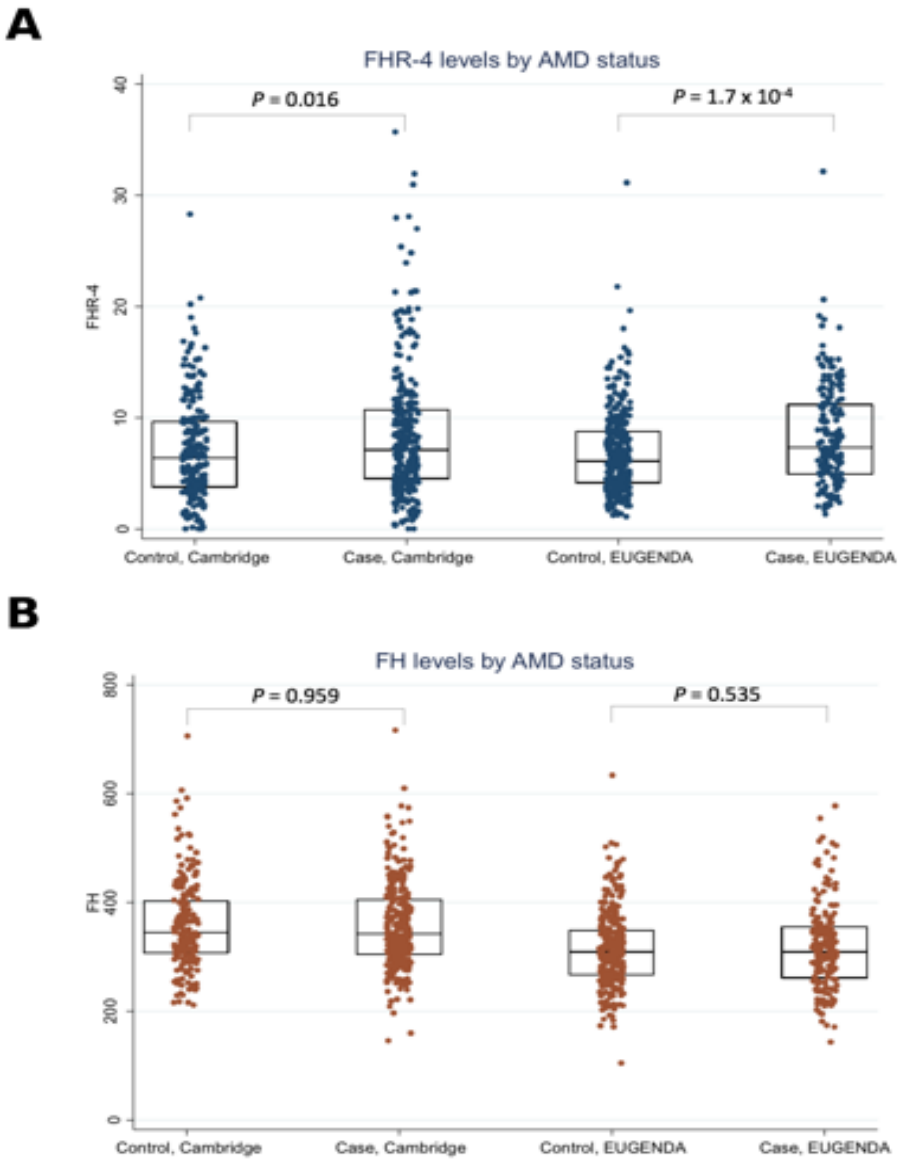

34

Figure 2

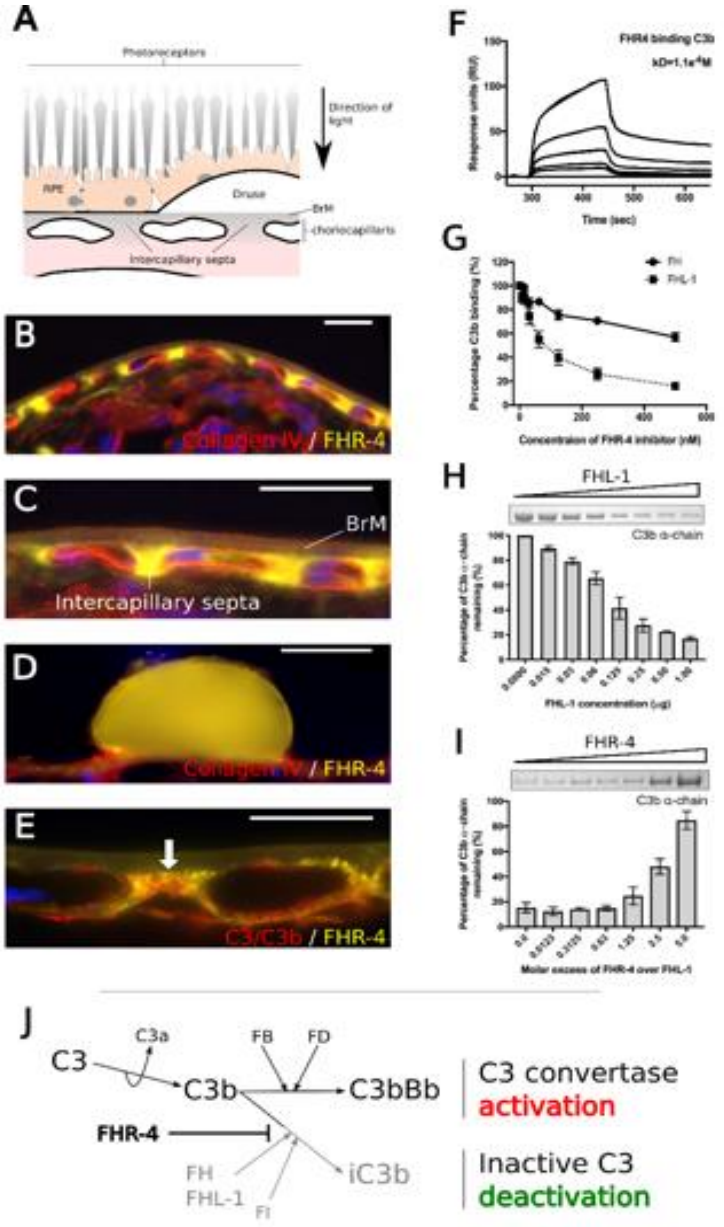
A
Photoreceptors
Direction of light
RPE
Drusen
BrM
Choriocapillaris
Intercapillary septa
B
Collagen IV / FHR-4
C
BrM
Intercapillary septa
D
Collagen IV / FHR-4
E
C3/C3b / FHR-4
F
FHR4 binding C3b
Response units (RU)
Time (sec)
G
FH
FHL-1
Percentage C3b binding (%)
Concentration of FHR-4 inhibitor (nM)
H
FHL-1
C3b α-chain
FHL-1 concentration (μg)
I
FHR-4
C3b α-chain
Molar excess of FHR-4 over FHL-1
J
C3
C3a
C3b
FB
FD
C3bBb
FHR-4
FH
FHL-1
FI
iC3b
C3 convertase activation
Inactive C3 deactivation

Figure 3

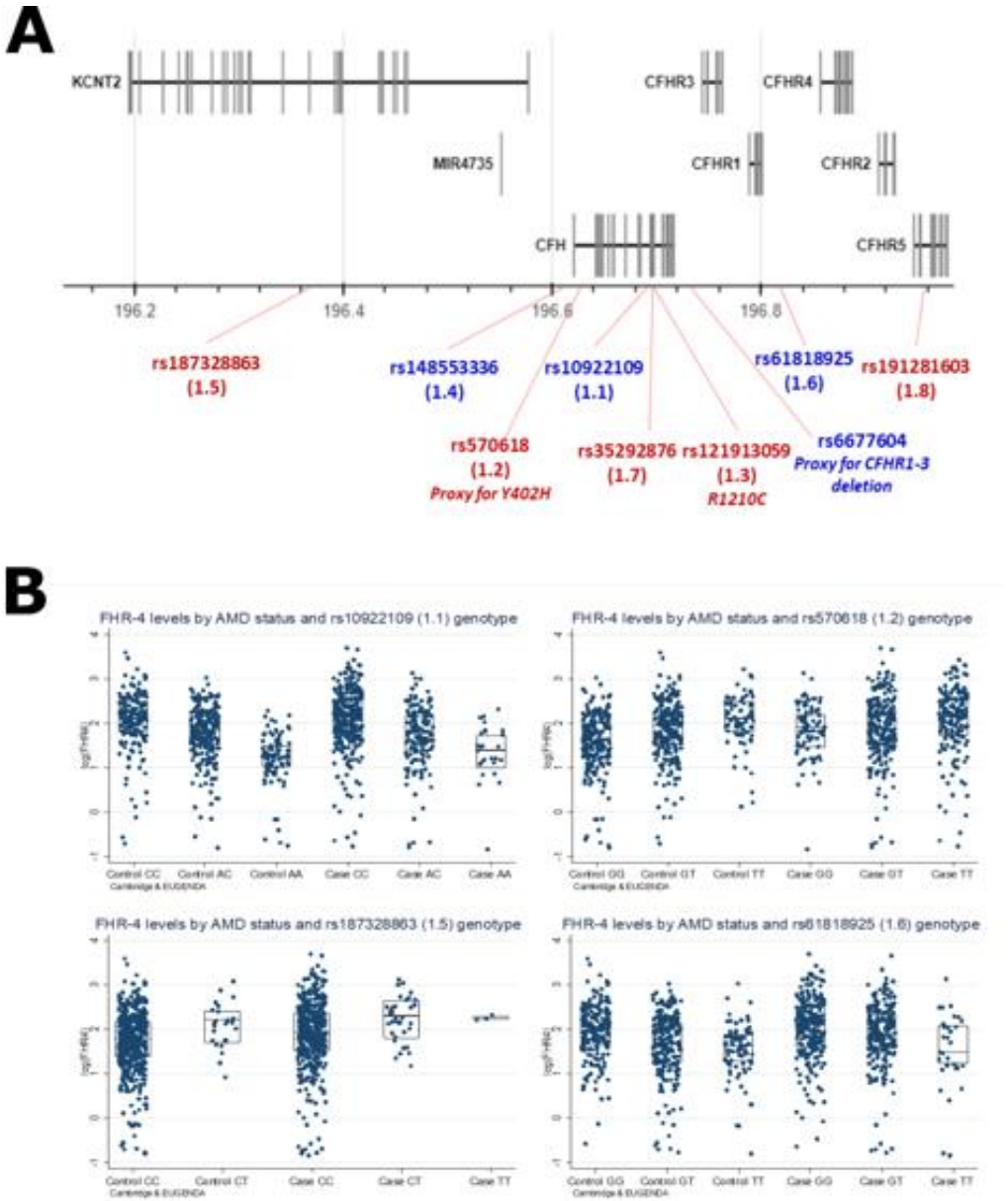
A
KCNT2
MIR4735
CFHR3
CFHR4
CFHR1
CFHR2
CFH
CFHR5
196.2
196.4
196.6
196.8
rs187328863
(1.5)
rs148553336
(1.4)
rs10922109
(1.1)
rs61818925
(1.6)
rs191281603
(1.8)
rs570618
(1.2)
Proxy for Y402H
rs35292876
(1.7)
rs121913059
(1.3)
R1210C
rs6677604
Proxy for CFHR1-3
deletion
B
FHR-4 levels by AMD status and rs10922109 (1.1) genotype
FHR-4 levels by AMD status and rs570618 (1.2) genotype
FHR-4 levels by AMD status and rs187328863 (1.5) genotype
FHR-4 levels by AMD status and rs61818925 (1.6) genotype

Figure 4

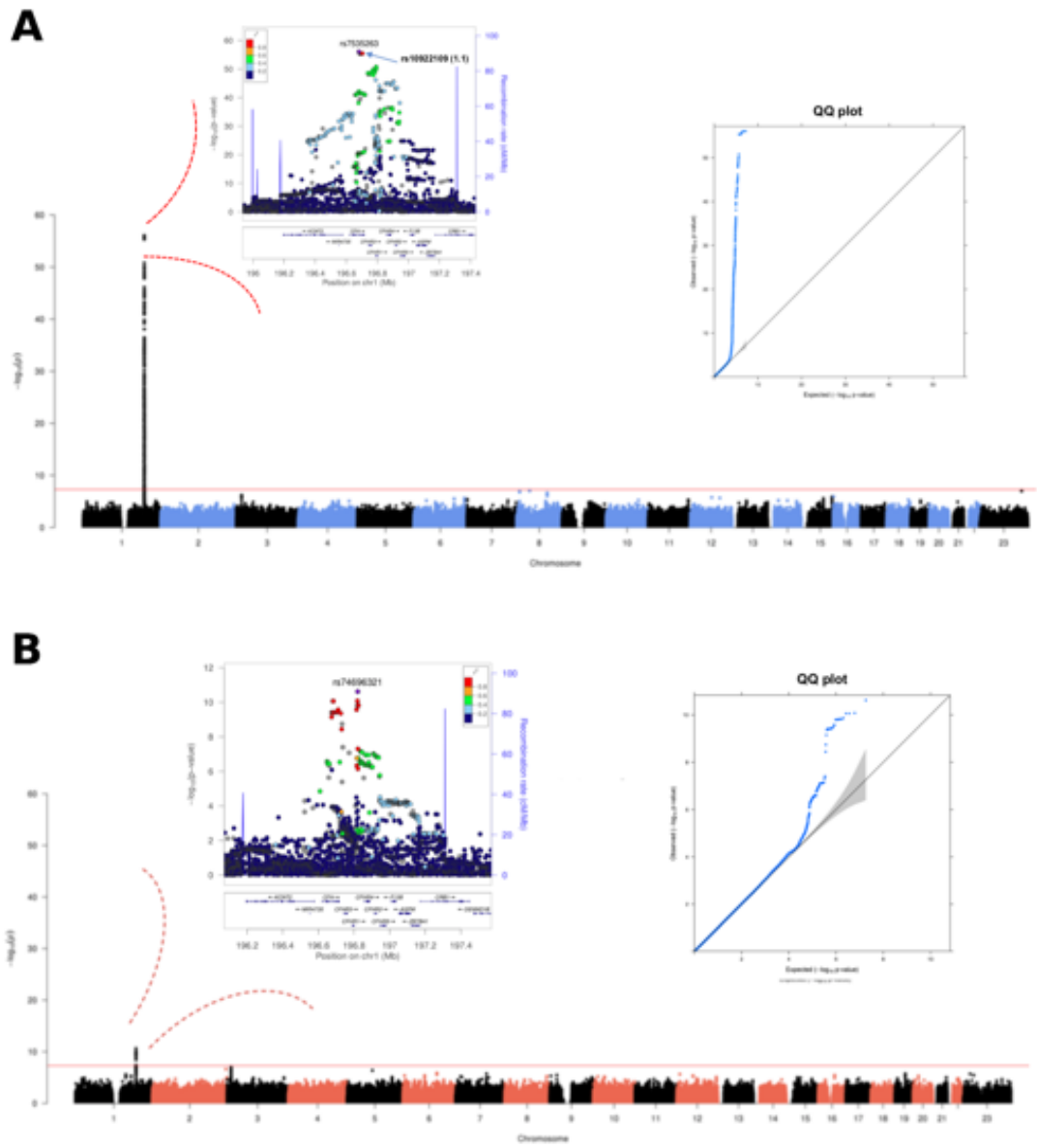

Figure 5

A

B

IAMDGC association signal number	1.5	1.4	1.2		1.1	1.7	1.6	1.8				
Major/Minor alleles	C/T	T/C	G/T	G/A	C/A	C/T	G/T	C/G				
(Direction)	(+)	(-)	(+)	(-)	(-)	(+)	(-)	(+)	Cambridge and EUGENDA		IAMDGC study	
Haplotype	rs1872328863	rs148453536	rs570618	rs6677604	rs10922109	rs35292876	rs61818925	rs191281603	Haplotype frequency		Haplotype frequency	
									Controls	Cases	Controls	Cases
H1	C	T	T	G	C	C	G	C	0.319	0.511	0.323	0.493
H2	C	T	G	G	A	C	T	C	0.229	0.119	0.216	0.117
H3	C	T	G	A	A	C	G	C	0.180	0.074	0.181	0.084
H4	C	T	G	G	C	C	T	C	0.125	0.127	0.120	0.121
H5	C	T	G	G	C	C	G	C	0.081	0.073	0.085	0.075
H6	T	T	T	G	C	C	G	C	0.024	0.041	0.024	0.051
H7	C	T	G	A	A	C	T	C	0.023	0.017	0.031	0.021
H8	C	T	T	G	C	C	T	C	0.013	0.018	0.011	0.017
H9	C	T	T	G	C	T	G	C	0.006	0.020	0.009	0.021

Most common haplotype CTTGCCGC (H1) that carries the disease risk allele of the proxy for Y402H (1.2) used as reference H1-H9 account for 98.5% of 2,012 chromosomes in Cambridge and EUGENDA

Figure 6

A

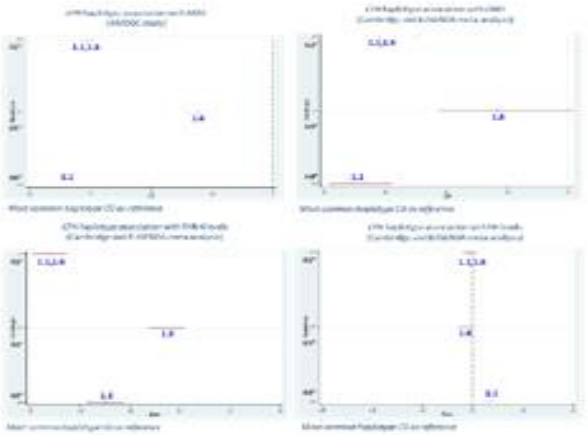

B

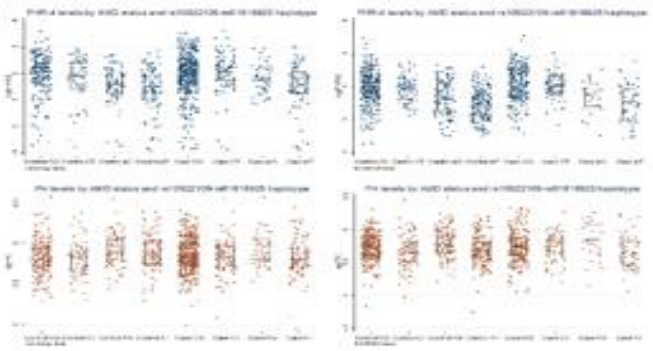

C

IAMDGC association signal number	1.1	1.6				
Major/Minor alleles	C/A	G/T	Cambridge and EUGENDA		IAMDGC study	
(Direction)	(-)	(-)				
Haplotype	rs10922109	rs6518925	Haplotype frequency		Haplotype frequency	
			Controls	Cases	Controls	Cases
H1*	C	G	0.136	0.61	0.111	0.638
H2*	A	T	0.248	0.136	0.243	0.137
H3*	C	T	0.135	0.147	0.129	0.139
H4*	A	G	0.181	0.076	0.184	0.086

*Most common haplotype CG (A+T *) used as reference